Hydroclimatic variability of opposing late Pleistocene climates in the Levant revealed by deep Dead Sea sediments

Yoav Ben Dor[1], Francesco Marra[1,2], Moshe Armon[1], Yehouda Enzel[1], Achim Brauer[3,4], Markus Julius Schwab[3], Efrat Morin[1]

[1] The Fredy and Nadine Herrmann Institute of Earth Sciences, The Hebrew University of Jerusalem, Jerusalem, 9190501, Israel

[2] Institute of Atmospheric Sciences and Climate, National Research Council of Italy, Bologna, 40129, Italy

[3] Section Climate Dynamics and Landscape Evolution, GFZ German Research Centre for Geosciences, Telegrafenberg, 14473, Potsdam, Germany

[4] Department of Earth Sciences, Potsdam University, Karl-Liebknecht-Straße 24/25, 14476, Potsdam, Germany

Correspondence to: Yoav Ben Dor (Yoav.Bendor1@mail.huji.ac.il)

Abstract. Annual and decadal-scale hydroclimatic variability describes key characteristics embedded into climate insitu, and is of specifically prime importance in subtropical regions. The study of hydroclimatic variability is therefore crucial to understand its manifestation as climate derivatives such as hydrological phenomena and water availability. However, the study of this variability from modern records is limited due to their relatively short span, whereas model simulations relying on modern dynamics could misrepresent some of its aspects. Here we study annual to decadal hydroclimatic variability in the Levant using two sedimentary sections covering ~700 years each, from the depocenter of the Dead Sea, which has been continuously recording environmental conditions since the late Pleistocene. We focus on the two series of annually deposited laminated intervals (i.e., varves) representing two episodes of opposing mean climates, deposited during lake level rise and fall at 27 and 18 Ka, respectively. These two series comprise alternations of authigenic aragonite that precipitated during summer and flood-borne detrital laminae deposited by winter floods. Within this record, aragonite laminae form a proxy of annual inflow and the extent of epilimnion dilution, whereas detrital laminae comprise sub-laminae that record individual flooding events. The two series depict distinct characteristics with increased mean and variance of annual inflow and flood frequency during "wetter", with respect to the "dryer", conditions, reflected by opposite lake level changes. In addition, decades of intense flood frequency are identified (e.g., clusters), depicting the insitu impact of shifting centennial-scale climate regimes, which are particularly pronounced during wetter conditions. The combined application of multiple time series analyses suggests that the studied episodes are characterized by weak and non-significant periodic components of sub-decadal frequencies. Combining these observations with the modern synoptic-scale hydroclimatology suggests that Pleistocene climate changes resulted in shifts of the dominance of the key synoptic systems that govern rainfall, annual inflow and flood frequency in the eastern Mediterranean over centennial time-scales.

1 Introduction

Human activity relies on continuous availability of freshwater, which in turn depends on the interaction of climatic, environmental and hydrologic processes. Water availability is particularly crucial in drylands and subtropical regions that cover significant portions of the Earth's surface and host nearly 20% of the world's population (e.g., Safriel et al., 2005). In these areas, hydroclimatic variability at seasonal, annual and decadal scales bear significant impact on water availability that could result in growing water stress as populations grow (e.g., Luck et al., 2015; Luo et al., 2015). It is therefore crucial to understand how hydroclimatic variability in drylands and Mediterranean regions could be affected by climate changes, as humanity faces in the upcoming decades (Peleg et al., 2015; Seager et al., 2019; Zappa et al., 2015; Ipcc, 2021). However, because the study of hydroclimatic variability requires high resolution measurements, that currently only cover several decades, the interpretation and the quantification of relationships between trends, oscillations and transition between climatic states, as well as their impact on the local water cycle insitu, are still limited and are therefore debated (e.g., Morin, 2011; Serinaldi et al., 2018). Furthermore, the impacts of climate change on short-term phenomena such as individual storms and floods, which bear substantial influence on the insitu water cycle in Mediterranean regions, are harder to determine from the available short historical records because the extent of available data does not adequately capture the full diversity of possible hydroclimatic states (Armon et al., 2018; Greenbaum et al., 2010; Tarolli et al., 2012; Metzger et al., 2020). Because palaeohydrologic archives often record centennial and millennial intervals at various resolutions (e.g., Allen et al., 2020; Baker, 2008; Brauer et al., 2008; Redmond et al., 2002; Witt et al., 2017), they have the potential to improve our understating of how climate change is manifested locally into short-term hydroclimatic variability (e.g., Ahlborn et al., 2018; Swierczynski et al., 2012). Nevertheless, this requires continuous high-resolution archives, which are rare, especially in sub-tropical arid terrestrial environments (e.g., Zolitschka et al., 2015).

The subtropical Levant exhibits a sharp climatic gradient ranging from subhumid Mediterranean in the north (Köppen-Geiger classification), where precipitation is focused in winter months (December-May), to hyperarid climate zones in the south (N-S; Kottek et al., 2006), and summers (June-September) are dry and hot . Because the main source of moisture to the region is the Mediterranean Sea, the orographic effect of the central mountainous belt of Israel results in an abrupt W-E climatic gradient, where the eastern parts are substantially drier than its eastern parts (Fig. 1; Kushnir et al., 2017). Under these seasonal conditions, the region is sensitive to spatiotemporal changes in global circulation, where slight modifications could bear substantial impact on the hydrological cycle and water availability (Fig. 1; e.g., Held and Soden, 2006; Luck et al., 2015; Shohami et al., 2011; Tamarin-Brodsky and Kaspi, 2017; Drori et al., 2021). The interaction of substantial seasonality and the abovementioned climatic gradients (N-S and E-W) over the eastern Mediterranean further obscure the impacts of climatic changes on intra- and inter-annual hydroclimatic variability in the wetter Mediterranean regions, as they ultimately stem from the frequency and properties of discrete extra-tropical Mediterranean cyclones (i.e., Mediterranean\Cyprus Lows\Cyclones; e.g., Campins et al., 2011; Enzel et al., 2003; Flocas et al., 2010; Saaroni et al., 2010; Ziv et al., 2004; Armon et al., 2020).

In this study, two high-resolution sequences of annually-deposited laminations (i.e., varves) of the Dead Sea deep drilling project (DSDDP) obtained from the Dead Sea depocenter within the framework of the international continental scientific drilling program (ICDP; e.g., Neugebauer et al., 2014) are analyzed to determine hydroclimatic variability in the southern

70 Levant under contrasting late Pleistocene global and regional climate changes, recorded by independently-determined lake level trends (i.e., mean "wetter" vs. "dryer" conditions; Fig. 2; e.g., Bartov et al., 2003; Torfstein et al., 2013a; Torfstein and Enzel, 2017). Two laminated segments were continuously sampled for thin-sections preparation, and analyzed using microfacies analyses in high-resolution and multiple time-series analyses in order to address the following questions: (a) Can any significant differences between the two studied episodes recording opposing climatic trends be identified? (b) Do the series

75 depict significant intra-series transitions indicative of hydroclimatic regime shifts? (c) Do the studied sequences (or parts of them) record any periodic components of spectral bands (e.g., interannual, decadal, multi-decadal components)? (d) Do the identified periodic components (partially) resemble the periodicity of known global teleconnection patterns (e.g., the North Atlantic Oscillation, NAO; Seager et al., 2019; Black, 2012)? i.e., can aspects of the modern hydroclimatic variability assist in interpreting dominant aspects of hydroclimatic variability during past climate changes such as periodic components?

80
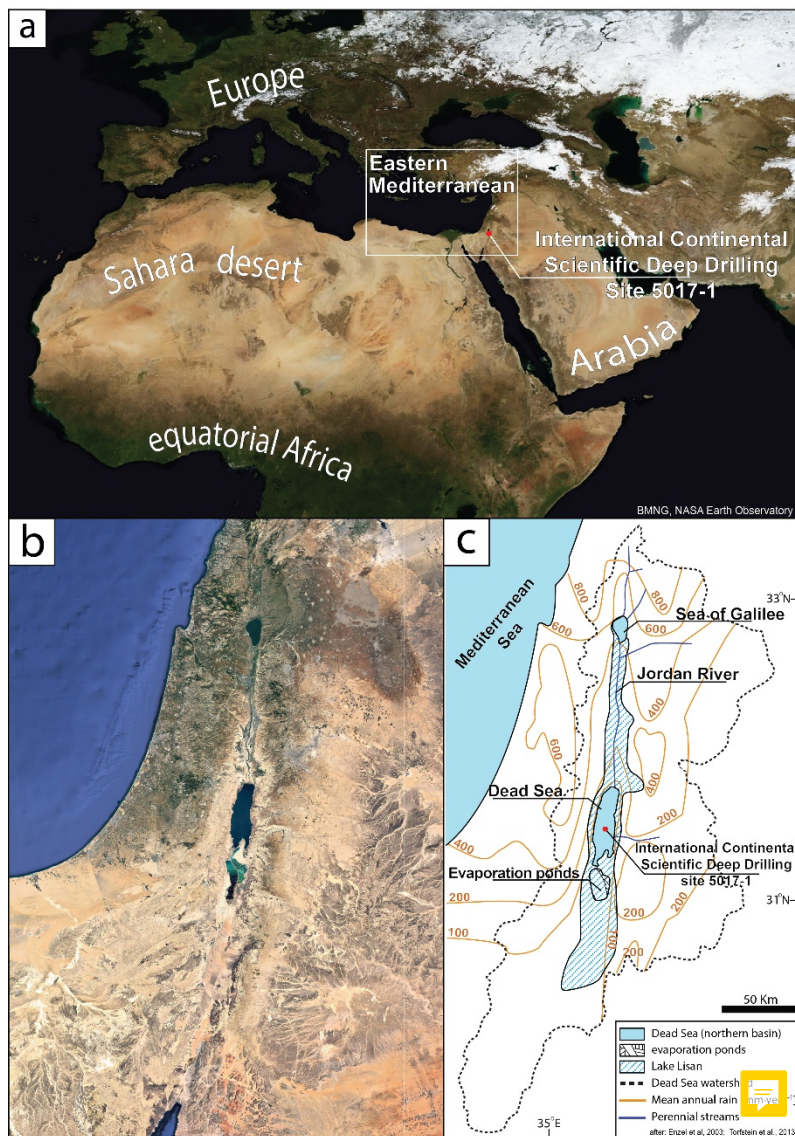
Figure 1 - a) Satellite image of the Mediterranean and its surroundings depicting the pivotal location of the ICDP-DSDDP site 5017-1 on the seam of global climate belts (extracted from The Blue Marble Next Generation, NASA's Earth Observatory; Stöckli et al., 2005). b) Satellite image of the eastern Mediterranean depicting the sharp climatic gradient between the Mediterranean north (mean annual precipitation >1000 mm·yr⁻¹) and the hyper-arid south (mean annual precipitation <50mm·yr⁻¹; image extracted from Google Earth). c) The Dead Sea watershed and the extent of Lake Lisan during the last glacial maximum (lake level ~170 m bmsl; ~260 m above modern level) with modern mean annual precipitation (after Enzel et al., 2003; Torfstein et al., 2013a).

85

2 Geological, hydrological, and climatological settings

90   The Dead Sea is the recent modern member of a series of waterbodies filling the deepest terrestrial depression on earth along the central part of the Dead Sea transform since the late Miocene (e.g., Garfunkel, 1981; Garfunkel and Ben-Avraham, 1996; Waldmann et al., 2017). Because changes Dead Sea level are directly linked to precipitation fluctuations over its watershed (e.g., Morin et al., 2019), its reconstructed lake levels are utilized as a "mega palaeo-rain gauge" (Enzel et al., 2003), recording the integrated impacts of environmental and climatic conditions on watershed hydrology (Bartov et al., 2003; Bookman et al.,

95   2006; Machlus et al., 2000; Torfstein and Enzel, 2017). These impacts are propagated into the lake's sedimentary record and are reflected by lithological transitions from sequences of alternating aragonite and detrital laminae that are deposited during high lake stands and positive water budget (Fig. 2; e.g., Ben Dor et al., 2019; Neugebauer et al., 2014; Torfstein et al., 2013b), to halite (e.g., Palchan et al., 2017; Sirota et al., 2017) or gypsum during drawdowns and droughts (Torfstein et al., 2008).

100 Althogh the full wet season lasts from October to May, ~65% of precipitation over the Dead Sea watershed is limited to the mild and wet winters (December-February). At the northern, and wetter part of the region, >90% of precipitation is delivered by low pressure systems from the Mediterranean Sea (i.e., Mediterranean Lows), whereas during summer (June-August), large-scale atmospheric subsidence results in stable dry and hot conditions (Goldreich, 2012; Kushnir et al., 2017; Tyrlis et al., 2013; Kelley et al., 2012). On average, the northern and western parts of the Dead Sea watershed are characterized by increased

105 precipitation and lower temperatures, resulting in a pronounced climatic N-S gradient. The average temperatures during winter range between ~10 and ~20°C, whereas during summer, temperatures range from ~20 to ~35°C, in the northern and southern parts of the Dead Sea watershed, respectively (Israel Meteorological Service, 2021). Mean annual precipitation in the hyperarid region is under 50 mm·yr^{-1}, delivered during less than 10 rainy days, whereas in the mountainous region at the north, it exceeds 1000 mm·yr^{-1} and spread over more than 75 rainy days (Goldreich, 2012; Sharon and Kutiel, 1986). Precipitation over the

110 southern part of the Levant is characterized by substantial spatiotemporal variability, depicting scattered, spotty, and intense convective rain (Sharon, 1972). The few observed precipitation events in the southern arid parts are separated by prolonged dry intervals ranging from weeks to months. The pronounced orographic effect of the Judean mountains, which separate the Lower Jordan Valley from the Mediterranean Sea, substantially decreases rainfall as storms progress eastward towards the Dead Sea basin, thus resulting in a sharp E-W precipitation gradient, which decreases from >500 mm·yr^{-1} in Jerusalem to <100

115 mm·yr^{-1} at the Dead Sea, over less than 50 km. East of the Dead Sea, the mountainous topography of the Jordanian escarpment increases annual precipitation to over 400 mm·yr^{-1} at its highest parts (Fig. 1; Enzel et al., 2003) .

Available records indicate that the modern climatic gradients over the Dead Sea watershed was similar during the late Pleistocene (Keinan et al., 2019; Enzel et al., 2008). These observations determine water and sediment transport paths into the

120 lake, where the main water source is its Mediterranean climatic zone to the north (Fig. 1; e.g., Enzel et al., 2003; Ziv et al., 2006), where annual precipitation and water supply largely depend on the spatiotemporal properties and the frequency of

extra-tropical cyclonic systems during winter (i.e. Mediterranean Lows; Campins et al., 2011; Goldreich, 2004; Saaroni et al., 2010). Detrital sediments are delivered to the ICDP 5017 coring site at the depocenter of the Dead Sea lake primarily by flash floods from adjacent streams (e.g., Nehorai et al., 2013; Ben Dor et al., 2018), and debris flows (Ahlborn et al., 2018). Whereas floods are generally associated with Mediterranean Lows (Dayan and Morin, 2006; Kahana et al., 2002; Tsvieli and Zangvil, 2005), debris flows, are associated with active Red Sea troughs (e.g., Ahlborn et al., 2018; Ben David-Novak et al., 2004). More rarely, subtropical jet stream disturbances can also generate flash floods (i.e., Tropical Plumes; Armon et al., 2018; Enzel et al., 2012; Tubi and Dayan, 2014; Ziv, 2001). Thus, the deposition of alternating authigenic aragonite and detrital laminae, which dominate the record of Lake Lisan the late Pleistocene predecessor of the Dead Sea (~70-14 Ka; Begin et al., 1980; Katz et al., 1977; Kaufman, 1971), throughout the majority of marine isotope stage 2 (MIS2) was attributed to annual deposition under seasonal climate during high lake levels and wetter-than-modern conditions, which sufficed to replenish the lake with necessary bicarbonate to support aragonite precipitation during summer and deliver detrital sediments during winter (Begin et al., 1980; Ben Dor et al., 2019; Haase-Schramm et al., 2004), as was further confirmed by the comparison of laminae counting and radiometric dating (Prasad et al., 2004; Migowski et al., 2006). In Lake Lisan, winter inflow from its northern part was likely the dominant source of water and alkalinity, replenishing carbonate content in the carbonate-poor Dead Sea after aragonite precipitation took place during summer (Kolodny et al., 2005; Neev, 1963; Neev and Emery, 1967; Stein et al., 1997), whereas local floods in adjacent (ephemeral) streams delivered detrital sediments to the lake's depocenter (Nehorai et al., 2013).

Until recently, studies of the sedimentary record of the Dead Sea and its predecessors focused on available outcrops surrounding the lake (e.g., Bartov et al., 2003; Bartov et al., 2007; Stein et al., 1997; Prasad et al., 2004; Torfstein et al., 2008) as well as short cores of Holocene sequences (e.g., Heim et al., 1997; Migowski et al., 2006). The broad aspect of their implications was thus limited due to local conditions and depositional hiatuses that form when lake levels fell below the outcrop's altitude (Machlus et al., 2000; Torfstein et al., 2013b; Torfstein et al., 2009) or by wave erosion during episodes of rising lake level. In addition, these outcrops were accumulated on the lake's shelf, and they therefore reflect its shallow environment, whereas the deeper part of the lake remained nearly inaccessible except for short coring campaigns (e.g, Garber et al., 1987; Nissenbaum et al., 1972). The recently collected ICDP-DSDDP cores from the lake's depocenter (ICDP site 5017), therefore, provide a new regional perspective on sedimentary, limnological and hydrological processes in the lake (Fig. 1; e.g., Coianiz et al., 2019; Neugebauer et al., 2014). The 5017 cores were dated by combining ^{14}C dating of macro organic debris including seeds and twigs (Neugebauer et al., 2014) with U-Th dating of primary aragonites (Torfstein et al., 2015), and by correlating their $\delta^{18}O$ with cave deposits (e.g., Lisiecki and Raymo, 2005; Bar-Matthews et al., 1999; Bar-Matthews et al., 2003). The age-depth model of the sections used in this study was established through a Markov chain Monte Carlo procedure utilizing ^{14}C dates covering ~50 Ka (Fig. 2; Kitagawa et al., 2017).

155 More recently, a detailed microfacies investigation revealed that the detrital laminae of the alternating aragonite and detritus facies, are comprised of multiple sub-laminae, recording individual flooding events from adjacent streams that face the 5017 ICDP coring site (Ben Dor et al., 2018). Because the majority of these streams are ephemeral, and have relatively small watersheds (<1000 km^2), such flash-floods may be triggered either by regional storms, that substantially contribute to the lake's annual water budget, and/or by smaller-scale local convection that has negligible impact on annual inflow. The laminated

160 sections of the ICDP-DSDDP core therefore provide a regional record of two (nearly) independent hydroclimatological variables at annual resolution: (a) the thickness of aragonite laminae (this study), and (b) the number of sub-laminae within detrital layers (Fig. 2; Ben Dor et al., 2018). Although more recent investigations indicate that aragonite laminae thickness is not linearly related to total annual inflow, as was previously suggested (Stein et al., 1997), it is correlated and monotonously associated with carbonate inflow and lake dilution, where increased inflow would result in increased aragonite thickness, and

165 may therefore still provide valuable insights on inherent periodicities and inter-annual inflow variability (Ben Dor et al., 2021).

  The alkalinity required to support annual aragonite precipitation may be derived from dust settling directly on the lake and its watershed, as well as freshwater inflow. However, direct dust deposition is insufficient to support the deposition of aragonite laminae (e.g., Ganor and Foner, 1996; Kalderon-Asael et al., 2009), whereas the dissolution and remobilization of accumulated

170 dust from the watershed, has the potential to supply bicarbonate that could increase inflow alkalinity (e.g., Crouvi et al., 2017; Belmaker et al., 2019). Although this cannot be directly addressed for MIS2, recent studies of the snow-affected Mt. Hermon region in Israel (Avni et al., 2018) and the denudation rates in the Judea region (Ryb et al., 2014), suggest that the dissolution of bedrock could not have increased alkalinity inflow by a factor greater than two, that would bear a more substantial impact on the northern part of the watershed. Thus the water and alkalinity budgets of the lake are ultimately dominated by rainfall

175 over the northern part of the watershed (~75-85%), and subsurface inflow (~10-15%; Siebert et al., 2014; Levy et al., 2020), whereas the water (and alkalinity) contribution of floods is negligible (5-10%; Armon et al., 2019). Because the number of detrital sub-laminae, on the other hand, records the number of floods exceeding a threshold and reaching the coring site that deliver negligible water volumes (Ben Dor et al., 2018), the two series are addressed in this study independently in order to examine their properties and interactions. Thus, although floods over the small watersheds draining into the Dead Sea deliver

180 both water and alkalinity into the Dead Sea (e.g., Belmaker et al., 2016; Golan et al., 2017), their overall negligible volume with respect to the annual inflow, makes the two studied proxies of aragonite thickness (this study) and the previously published number of detrital sub-laminae (Ben Dor et al., 2018) practically independent.
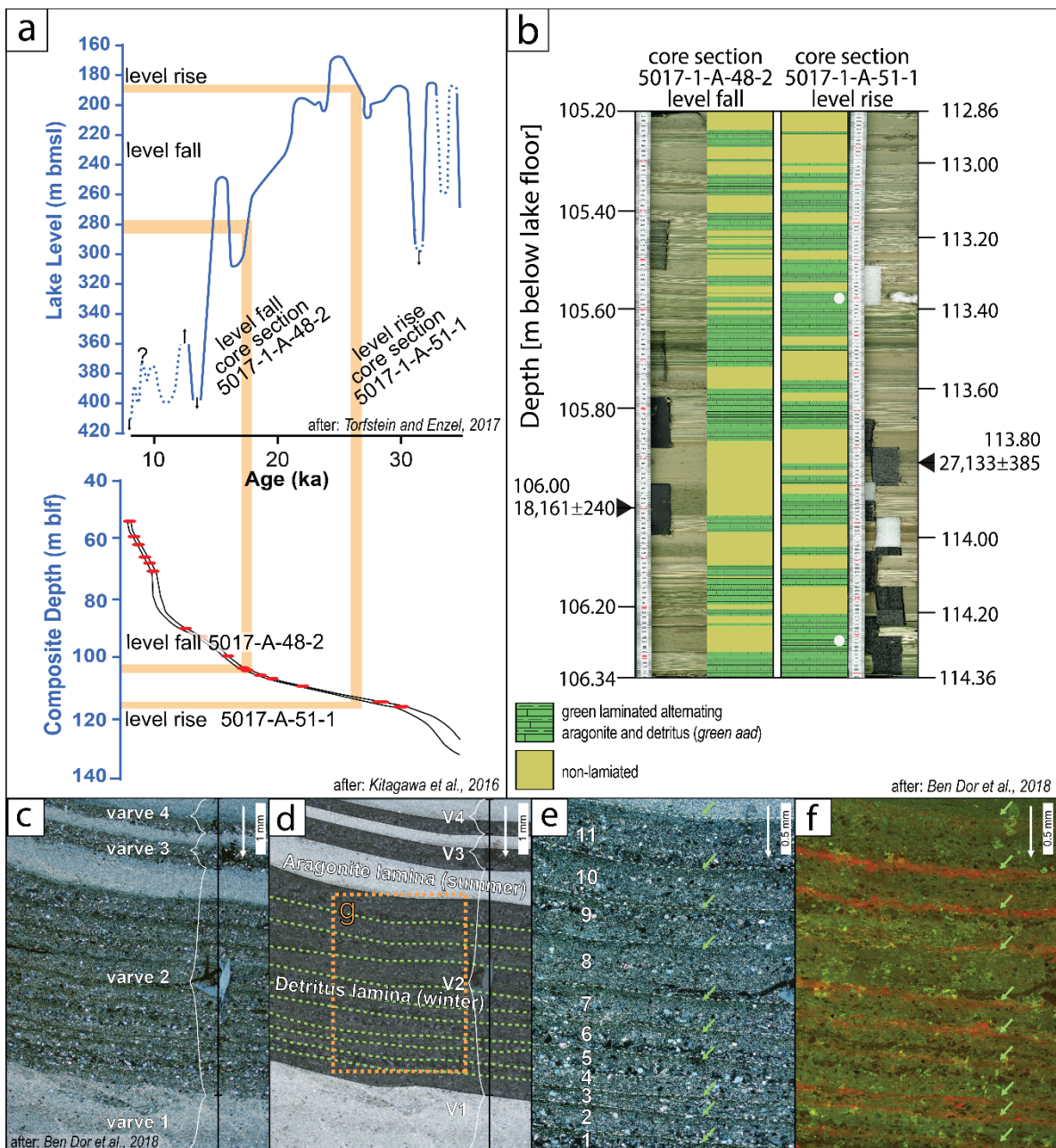
185

Figure 2 - a) Top: Dead Sea lake level depicting the highest stage of Lake Lisan during last glacial maximum, the Late Pleistocene predecessor of the Dead Sea (Bartov et al., 2003; Torfstein and Enzel, 2017). Bottom: The age-depth model of the ICDP-DSDDP 5017-1 core and the position of the studied segments along the core (after Kitagawa et al., 2017). b) The studied sections of the ICDP-DSDDP cores dated to 18 Ka and 27 Ka (marine isotope stage; MIS2, ~15-30 Ka). c-f) Microscope images of alternating aragonite
190 **(summer precipitate) and detritus (deposited during winter) varves depicting a detrital laminae composed of multiple sub-laminae (labelled 1-11) deposited by individual floods (after Ben Dor et al., 2018).**

3 Materials and methods

3.1 Microfacies analyses

195 Two chronologically-constrained segments (each ~1.5 meter long) of the ICDP-DSDDP 5017-1 core deposited during ~18 and 27 Ka were selected for this study (Fig. 2; Neugebauer et al., 2014). These segments are coeval with opposing climatic trends, reflected by independently-determined rising (27 Ka) and falling (18 Ka) lake level trends (Bartov et al., 2002; Torfstein and Enzel, 2017). The two sections were sampled continuously with overlap to prepare sequence comprising 10 cm long thinsections using a dry-freeze procedure adjusted for saline sediments (e.g., Brauer et al., 1999; Neugebauer et al., 2015), and

200 analyzed using a Hirox RH-2000 optical microscope (e.g., Ben Dor et al., 2018; Ben Dor et al., 2021). A total of ~700 varves (years) were counted and described in each segment. The segments comprise alternations of finely laminated varves (Ben Dor et al., 2019) and event-related deposits (Neugebauer et al., 2014), attributed to debris flows (Ahlborn et al., 2018) and earthquakes (Fig. 2; Kagan et al., 2018). The nature of these sediments and the way their mode of formation according based on the study of available exposures (Begin et al., 1980; Begin et al., 1974; Stein et al., 1997; Marco et al., 1996), and modern

205 analogous lakes (e.g., Dean et al., 2015; Roeser et al., 2021) suggest that these detritus-aragonite couplets were deposited annually, thus forming varves. This is further supported by the uniformity of the sediments revealed by microfacies analyses carried out in this study, in which slight changes sediment properties are observed in detail and the agreement between laminae counting and independent radiometric dating such as ^{14}C and U-Th (Prasad et al., 2009; Haase-Schramm et al., 2004; Neugebauer et al., 2015). Because no deposition of alternating aragonite and detritus sedimentary facies takes place under

210 modern conditions in the Dead Sea (e.g., Ben Dor et al., 2021), the interpretation of alternating aragonite and detritus facies as annual deposits is a relatively solid assumption used within the framework of this study, as it cannot be directly determined for the studied interval Lake Lisan (e.g., Prasad et al., 2004; Ben Dor et al., 2019; Ben Dor et al., 2020).

This study focuses on two properties of the varves interpreted as hydrological proxies: (a) the number of detrital sub-laminae

215 in each detrital lamina (Ben Dor et al., 2018), and (b) the thicknesses of aragonite laminae (this study). Because the thickness of detrital laminae (Fig. 2) is not directly linked to specific hydroclimatic processes, but instead depends on the interaction of multiple factors such as sediment availability and the geographical position of the activated catchment, it is not analyzed here as a hydroclimatic proxy. The thickness of aragonite laminae was suggested to reflect annual inflow and lake dilution during the wet season (Kolodny et al., 2005; Stein et al., 1997), whereas individual sub-laminae in detrital laminae correspond to

220 flood events capable of delivering siliciclastic sediments to the coring site (Ben Dor et al., 2018). These sub-laminae are attributed to floods that surpassed the threshold required to reach the coring site from their catchments. Missing data where laminae are trimmed or distorted (~5%) were imputed using singular spectrum analysis (e.g., Kondrashov and Ghil, 2006).

Because the typical number of sub-laminae is low, and the minimal number of detrital sub-laminae that can be counted is one,

225 as no cases of "zero sub-laminae" are sedimentologically-distinguishable, varves comprising a single detrital lamina should

be considered as varves recording either years with no floods or years with a single flood. The two series deposited during rising and falling lake levels were compared using key statistical properties: the Mann-Whitney-Wilcoxon ranksum test to determine if they were sampled from two populations of a statistically different median (MWW; Mann and Whitney, 1947), and the Ansari-Bradley ranksum dispersion test (AB; Ansari and Bradley, 1960) to determine if they were characterized by statistically significant dispersion.

3.2 Detecting intra-record regime shifts

A non-parametric test was developed in order to identify regime shifts as part of this study by comparing the observed running sum of sub-laminae count normalized by its mean value using consecutive multiple window widths ranging from 10 to 300 years, against the surrogate series generated by point-wise permutations of the data (Eq. 1; Figs. 3 and S1-S5).

$$\text{Eq. 1:}\quad y_{w(i)} = \begin{cases} i < \frac{w}{2} & NaN \\ \frac{w}{2} < i < N - \frac{w}{2} & \frac{\sum n_j}{\widehat{y_w}}, \left[i - \frac{w}{2} \leq j \leq i + \frac{w}{2}\right] \\ i > N - \frac{w}{2} & NaN \end{cases}$$

Equation 1 - the normalized running sum of sub-laminae counts. $y_{w(i)}$ is the normalized running sum, i is the location index ranging between 1 and N, N is the number of data points in the studied series, $\sum n_j$ is the sum of sublaminae count over the range between $\left[i - \frac{w}{2} \leq j \leq i + \frac{w}{2}\right]$, w is the window width ranging from 10 to 300 by 10 years steps (w =[10,20,30,…,290,300]) , and $\widehat{y_w}$ is the mean normalized sum of n for window width w. The resulting $y_{w(i)}$ values larger than unity indicate flood-rich episodes, whereas $y_{w(i)}$ values lower than unity indicate flood-poor episodes.

Because the aim of this analysis is to assess the probability of observing decadal to centennial intervals of increased flood frequency (i.e., clustering of floods) whilst avoiding a-priori assumptions and parametrization, and because the two series depicts low serial dependence (Fig. S6), the surrogate time series were produced by point-wise permutations. After the running sum was normalized by its mean value for every window width, and local maxima values that are separated by at least half of the window width were considered for the analysis (Fig. 3c and 3d). The peaks were ranked in descending order and compared against a dataset derived from 10,000 permutations without replacement of the respective series, revealing the significance level of observing intervals of the studied window width. Observed values larger than the 95th percentile of the permutated series are considered statistically significant with a false positive error of α=0.05 (Fig. 3e and 3f). Because the significant peaks of different window widths overlap, the clusters were evaluated by considering their summed probabilities (Fig. 3g and 3h), and their edges were refined by the a running MWW and AB tests, in which the two halves of the window are compared against each other (Figs. S7-S8).
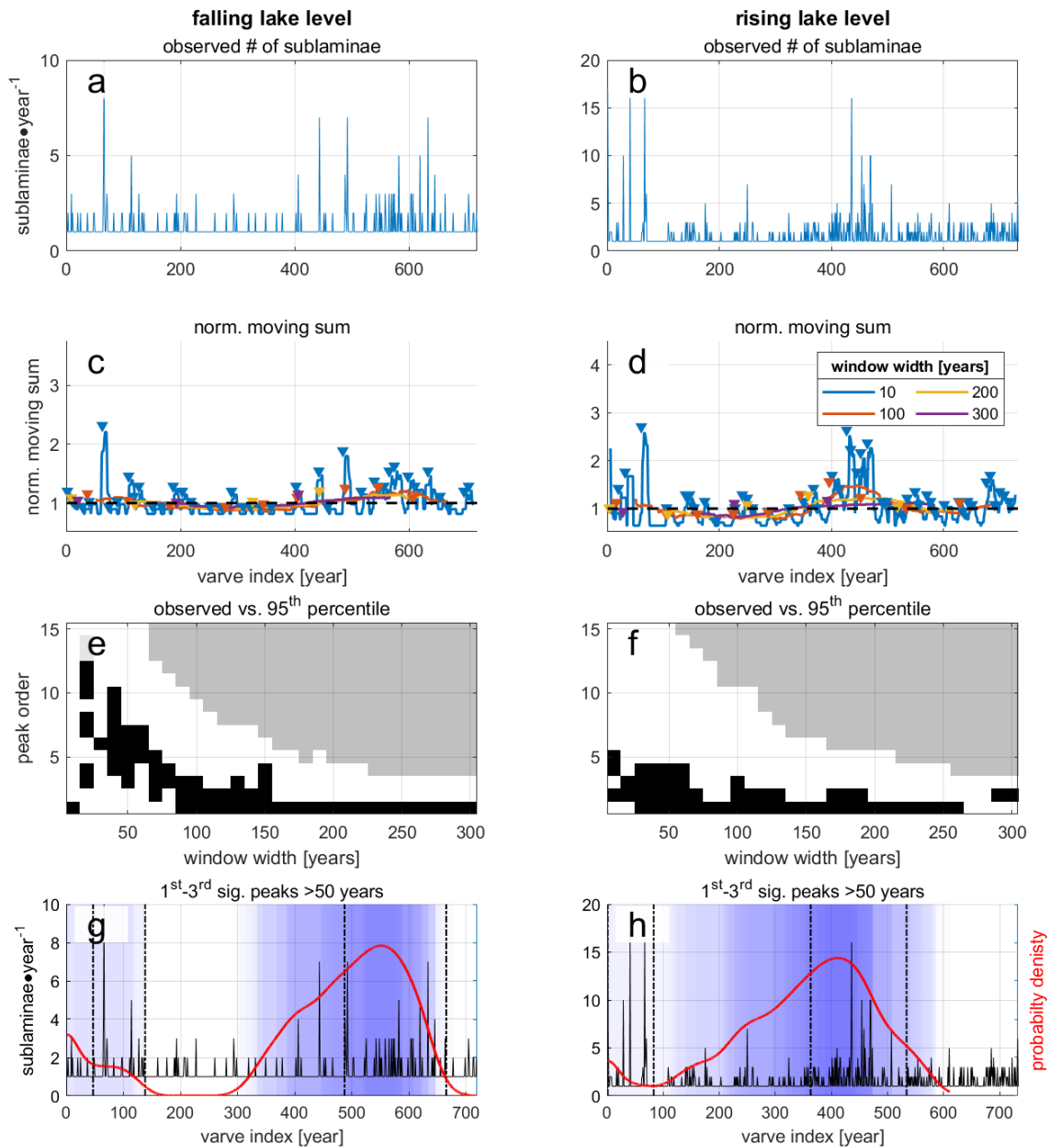
Figure 3: the non-parametric test developed for identifying flood-rich episodes (i.e., flood clustering) a,b) the studied series of flood frequency analyzed using microfacies analyses of two DSDDP core sections. c,d) the running normalized sum calculated for identifying flood clusters and its peaks (triangle) using different window widths. e,f) binary diagrams indicating where observed $y_{w(i)}$ values are higher than the calculated 95th percentile of the distributions derived from 10,000 randomly permuted series, and are thus statistically significant at α=0.05 (black pixels) or non-significant (white pixels). Missing values, where not enough peaks

Recurrence and joint-recurrence techniques and their analyses (*RQA* and *JRQA*) were applied to identify non-linear transitions and distinct regimes within the series (Eckmann et al., 1987). These methods can be used to detect abrupt transitions as well as short-term periodic and oscillatory behaviours in non-stationary and noisy data by investigating their dynamics in the reconstructed phase space (Donges et al., 2011; Marwan et al., 2007). The following short introduction and included equations are based on the detailed review by Marwan et al. (2007), to which the keen reader is referred for further details. The recurrence of the system is computed by considering the pairwise similarity (proximity) of points along its phase space trajectory reconstructed using a time delay (τ) and an embedding dimension (m). The recurrence plot (*RP*), which is used to efficiently visualize the recurrence of the studied series, is generated by calculating the $R_{i,j(\varepsilon)}$ matrix, through the binarization of the difference between the norm of the pairwise trajectories of steps in the reconstructed phase space using a predefined threshold ε (Eq. 2; Marwan et al., 2007). When the trajectory in two points (i and j) is smaller than ε, the value of the corresponding point is set to one in R, and the pixel painted black in the *RP*. Otherwise the value is set to zero and the corresponding pixel in the RP is painted white.

$$\text{Eq. 2:} \quad R_{i,j(\varepsilon)} = \theta\big(\varepsilon - \|\vec{x}_i - \vec{x}_j\|\big), \qquad i,j = 1,2,3,\dots,N$$

Equation 2 (after Marwan et al., 2007) – the calculation of the recurrence matrix using a threshold ε, where N is the number of points of the reconstructed $\vec{x}_i$ trajectory, and $\theta(\cdot)$ is the Heaviside function (step function), where $\theta(x) = 0$, if x<0 and $\theta(x) = 1$ otherwise.

Similarly, the joint recurrence plot can be derived (JRP) for studying the dynamical relationship of two series or more by the product of recurrence plots (Eq. 3; Romano et al., 2004).

$$\text{Eq. 3:} \quad JR_{i,j(\varepsilon_{\vec{x}},\varepsilon_{\vec{y}})} = \theta\big(\varepsilon_{\vec{x}} - \|\vec{x}_i - \vec{x}_j\|\big) \cdot \theta\big(\varepsilon_{\vec{y}} - \|\vec{y}_i - \vec{y}_j\|\big), \quad \vec{x}_i \in \mathbb{R}^m, \vec{y}_i \in \mathbb{R}^n, \; i,j = 1,2,3,\dots,N$$

Equation 3 (after Marwan et al., 2007) – the calculation of the joint recurrence matrix as the product of two recurrence matrices calculated for two series with trajectories $\vec{x}$ and $\vec{y}$, using the thresholds $\varepsilon_{\vec{x}}$ and $\varepsilon_{\vec{y}}$, respectively. N is the number of points of the trajectories, and $\theta(\cdot)$ is the Heaviside function (step function), where $\theta(x) = 0$, if x<0 and $\theta(x) = 1$ otherwise.

The *RP* of a cyclic system would show diagonal lines parallel to the line of identity (*LOI*), which connects its lower left corner with its upper right one, whereas a noisy system would be characterized by spotty and random appearance of points throughout the *RP*. Once the *RP* is calculated, its properties and the time dependent behaviour of the system can be studied by quantifying its recurrence using recurrence quantification analysis (*RQA*) by computing different measures for each sub-matrix formed by sliding a square window along its *LOI* with a predefined step. In this study the recurrence rate (*RR*), determinism (*DET*), the

maximum length of a diagonal line within a sub-matrix (L_{max}) and the laminarity (LAM) metrics are used. The maxima of DET and L_{max} can be used to identify periodic-chaos and chaos-periodic transitions. Alongside those transitions in LAM (minima), it is capable of identifying chaos-chaos transitions as well (maxima). The recurrence rate is the percentage of points in which recurrence occurs within the studied section (Eq. 4).

300 Eq. 4: $RR(\varepsilon) = \frac{1}{N^2} \sum_{i,j=1}^{N} R_{i,j}(\varepsilon)$

The determinism (DET) reflects the extent to which the system maintains an ordered, cyclic and deterministic behaviour. Because uncorrelated, weakly correlated, stochastic or chaotic processes form very short diagonals or none at all, whereas deterministic processes generate longer diagonals, the ratio of recurrence points that form diagonal lines (with length$\geq l_{min}$) to all recurrence points can be used to estimate the main behaviour of the system within the studied period (Eq. 5). In this study

305 the minimal length of l (l_{min}), was set to $l_{min} = 2$.

Eq. 5: $DET = \frac{\sum_{l=l_{min}}^{N} l\, P(l)}{\sum_{l=l}^{N} l\, P(l)}$

Similar to DET, the laminarity (LAM) is computed as the portion of points forming a vertical line of minimal length v out of the entire set of recurrence points within the RP (or in its sub-matrices).

Eq. 6: $LAM = \frac{\sum_{v=v_{min}}^{N} v\, P(v)}{\sum_{v=1}^{N} v\, P(v)}$

310 In order to decrease the influence of the tangential motion LAM is computed using the points forming v that exceed a minimal length v_{min}, set in this study as $v_{min} = 2$. In cases where the RP consists of more single recurrence points than vertical structures LAM will decrease.

The length of the longest diagonal line (L_{max}) is computed by identifying the longest diagonal line found within the RP (or in

315 its sub-matrices; Eq. 7).

Eq. 7: $L_{max} = \max\left(\{l_i\}_{i=1}^{N_l}\right)$

where $N_l = \sum_{l \geq l_{min}} P(l)$ is the total number of diagonal lines.

This approach is specifically useful in this study because the studied proxies record the convolved non-linear interaction of

320 climatic, hydrological and limnogeological processes, because the effect of their interactions could stem from non-linear dynamics that bear very different implications on sedimentary sections (Marwan and Kurths, 2004; Marwan et al., 2003). The analysis was carried out using the CRP toolbox for MATLAB© after normalizing the series to zero mean and unit standard deviation (ver. 5.22; Marwan et al., 2007). The embedding dimension and the time-delay were determined using the false nearest neighbour approach (Kennel et al., 1992) and the mutual information method (Fig. S6; Marwan, 2011). The threshold

325 ε was set to fit a recurrence rate (RR) of 0.1 using the max norm method (Schinkel et al., 2008), and the RQA (and JRQA) measures were calculated with a window of 30 years with a time step of a single year.

3.3 Detecting periodic components

Hydrological data are commonly skewed, and may exhibit short-term periodic behaviour that is difficult to identify using standard Fourier-derived approaches such as the periodogram (e.g., Blackman and Tukey, 1958; Welch, 1967). Wavelet 330 analyses provide a set of flexible tool for identifying irregular and non-stationary periodicities in short time series (Lau and Weng, 1995; Torrence and Compo, 1998). The coherence of two series provides an estimate of the importance of areas with high common power in the two series, that reflects the localized correlation coefficient in time-frequency space (Grinsted et al., 2004). Wavelet analyses were carried out using the Morlet wavelet function after normalizing the data to zero mean and unit standard deviation. The significance of the wavelet power and coherence were determined against red noise simulated 335 using a lag-1 autoregressive process (AR(1)) using the cumulative area-wise approach for detecting false positive periodicities at the α=0.05 (Schulte, 2019, 2016).

Singular spectrum analysis (SSA) is used to identify periodic and oscillatory signals in short, non-stationary and noisy time series (Broomhead and King, 1986). Unlike wavelet and Fourier-based procedures, where the signal is compared against a 340 predefined function, SSA identifies principle components that best explain the variance of the time-delayed series through the embedded matrix. This non-parametric approach reveals the dominant components that best explain the variance and defines their relative contribution for generating the observed signal (Vautard and Ghil, 1989). This, in turn, allows the breaking-down of the signal into its principle components and calculating their corresponding reconstructed components (RCs), which demonstrate the extent of contribution for each component to the signal (Ghil et al., 2002). Generally, SSA complements 345 wavelet and other spectral analyses because it provides increased flexibility, and may identify oscillatory components of different shapes that change in time. Thus, the analyses of the individual RCs, and the determination of their dominant periodic components can point at dominant frequencies embedded in the observed series, which in turn could stem from teleconnection patterns affecting hydroclimatic variability (e.g., NAO, SOI, etc.; Feliks et al., 2010; Le Mouël et al., 2019; Seager et al., 2019). In order to balance between the analyses complexity and usefulness, the SSA was performed with an embedding 350 dimension (window) of ten years after visually inspecting the effect of the number of RCs on the relevant eigenvalues. The first RC ($RC^{(1)}$) was later used as the local trend component that was subtracted from the data as a high-pass filter to reveal short-term periodicities (Fig. S9). The SSA RCs were additionally analyzed using the Welch periodogram for evaluating the RCs power spectral density (Welch, 1967), and wavelet analyses using the area-wise test for significance (Schulte, 2016, 2019) in order to compare their time-frequency properties during cluster and background periods. The Welch periodogram was 355 calculated after applying a Hamming window of width 25 years and an overlap of 50%, applied to merge close periodic components and reduce spectral noise, after subtracting the mean from the series and zero-padding it to 2^{11} points in order to minimize spectral leakage (Figs. S10-S13).

4 Results

4.1 Microfacies analyses

360   The studied segments are dominated by greenish alternating laminae of aragonite and detritus (Fig. 2) characterized by a typical laminae thickness of <1 mm. Detrital laminae are dominated by quartz, clay and organic matter, with some calcite, dolomite and feldspar grains, commonly showing graded bedding, a clay cap of and a thin lamina of amorphous organic matter (Fig. 2). The laminated segments are interrupted by massive or graded ERDs attributed to abrupt mass wasting events (e.g., turbidities and slumps), triggered by earthquakes (Kagan et al., 2018), debris flows and slope instability (Ahlborn et al., 2018). Both

365   laminae thickness and number of sub-laminae show statistically significant larger mean and variance during lake level rise (~27 Ka) than during lake level fall (~18 Ka; Table 1; Figs. 4 and 5).

    Aragonite laminae thicknesses range between 51 and 2,259 µm (µ=457µm, σ=308 µm), and 53 and 6,020 µm (µ=642 µm, σ=529 µm) in the falling and rising segments, respectively. Detrital laminae thicknesses range from 27 to 13,136 µm

370   (µ=312µm σ=638 µm), and 27 and 8,760 µm (µ=416 µm, σ=675 µm) in the falling and rising segments, respectively. The number of sub-laminae during the falling lake level ranges between 1 and 10 (µ=1.2, σ=0.7), and between 1 and 17 (µ=1.6, σ=1.6) in the rising lake level, respectively (Table 1). The MWW test indicates a significant difference between all studied proxies when comparing the two studied series (p value <<0.05). The difference in dispersions of all variables between rising and falling lake levels are statistically significant (p value<<0.05) except for detrital laminae, where the Ansari-Bradley test

375   failed to reject the null hypothesis (p value≈0.12). All three parameters show positive skewness of 2.1 µm and 3.5 µm for aragonite laminae thickness, 12.7 µm and 7.6 µm for detrital aragonite laminae, and 5.9 and 6.1 of sublaminae count during falling and rising lake levels, respectively. No significant correlation exists between any two of the parameters in each time series, with the exception of a moderate correlation between the number of sub-laminae in the detrital laminae and laminae thickness (Fig. 4; r=0.52 and 0.61, for falling and rising lake levels, respectively; with p values <<0.005).

380

Table 1 – Bulk statistical properties of the studied sedimentary series.

Rise/fall	Parameter	Unit	Min	Max	Median	Mean	Std. deviation	Skewness
fall	aragonite	µm	51	2,259	389	458	308	2.1
fall	detritus	µm	27	13,136	167	316	639	12.6
fall	number of detrital sub-laminae	count	1	10	1.0	1.2	0.7	5.9
rise	aragonite	µm	53	6,020	512	643	529	3.5

| rise | detritus | µm | 27 | 8,760 | 261 | 416 | 675 | 7.6 |
| rise | number of detrital sub-laminae | count | 1 | 17 | 1.0 | 1.6 | 1.6 | 6.1 |

Table 2 – p values of the statistical comparison between the bulk studied series

Parameter	Test[1]	p value[2]	Significant at α=0.05
aragonite	MWW	< 0.001	yes
detritus	MWW	< 0.001	yes
number of detrital sub-laminae	MWW	< 0.001	yes
aragonite	AB	0.001	yes
detritus	AB	0.248	no
number of detrital sub-laminae	AB	< 0.001	yes

385   1 – MWW – Mann-Whitney-Wilcoxon ranksum test, AB – Ansari-Bradley dispersion test.
     2 – tests with p values smaller than 0.05, are considered significant at α=0.05.
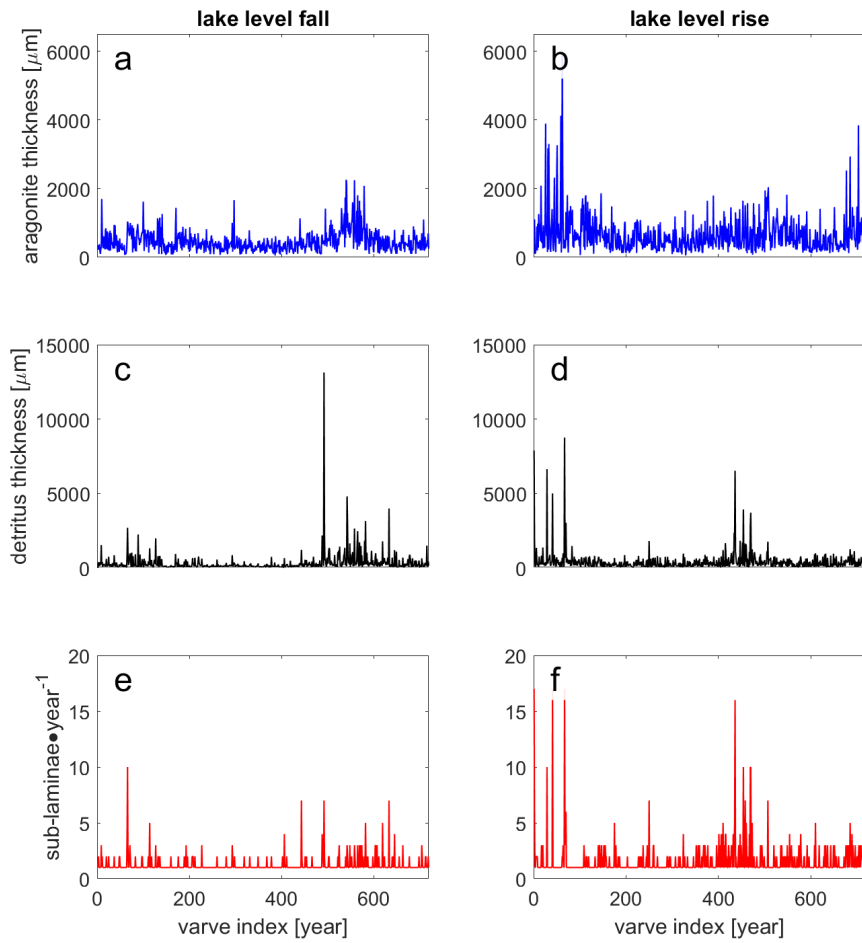
Figure 4 – Time series of microfacies analysis of the studied varved sections. (a, b; blue) aragonite laminae thickness, (c, d; black) detritus laminae thickness, (e, f; red) number of detrital sub-laminae.
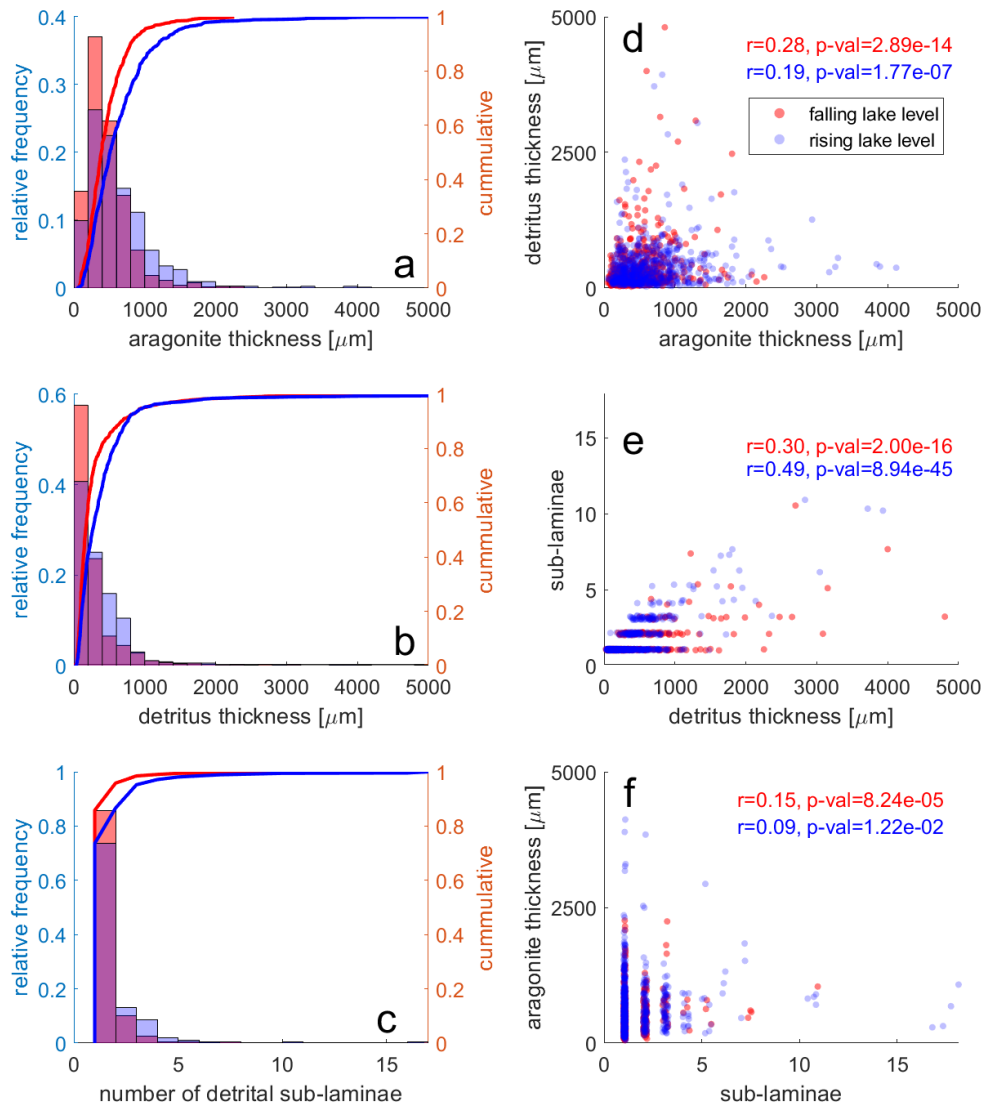
Figure 5 – Distributions and scatter plots of the trivariate geological time series showing the distributions of (a) aragonite laminae thickness, (b) detritus laminae thickness and c) number of sub-laminae counted in each detrital lamina. Plots d-f show the correlations between aragonite and detritus thickness (d, r^2=0.07, 0.03), number of floods and detritus thickness (e, r^2=0.27, 0.37), and number of floods and aragonite laminae thickness (f, r^2=0.03,0.01)

4.2 Detecting intra-record regime shifts

Two clusters of intense flood frequency were identified in each of the studied series (Fig. 3; Table 3). Although two clusters are identified, one of the clusters in each series appears more robust in comparison with the other, as it was identified using multiple window widths (Figs. S5), and the clusters are labelled as robust and less robust accordingly (Table 3). However, it is noted that this different robustness estimation could stem from an "edge effect" bias, that limits the analysis of segments close to the edges of the series when large window widths are applied. The RPs of aragonite series depict some short diagonal lines, whereas those of the sub-laminae show more spotty properties with blocky character (Figs. 6 and 7). An increase in both DET and L_{max} is identified close to the clusters' edges, although the RQA measures fluctuate throughout the series, and do not exhibit pronounced changes or trends with respect to the identified clusters. Both JRPs depict fairly low recurrence with spotty and patchy patterns, with some diagonal lines in the series of the falling lake level.

Table 3 – Identified clusters in the two studied series following the procedure Appendix B based on number of detrital sub-laminae.

	Level fall [index years]	Estimated robustness	Level rise [index years]	Estimated robustness
1st cluster	47-138	Less robust	1-83	Less robust
2nd cluster	487-662	Robust	363-534	Robust

410
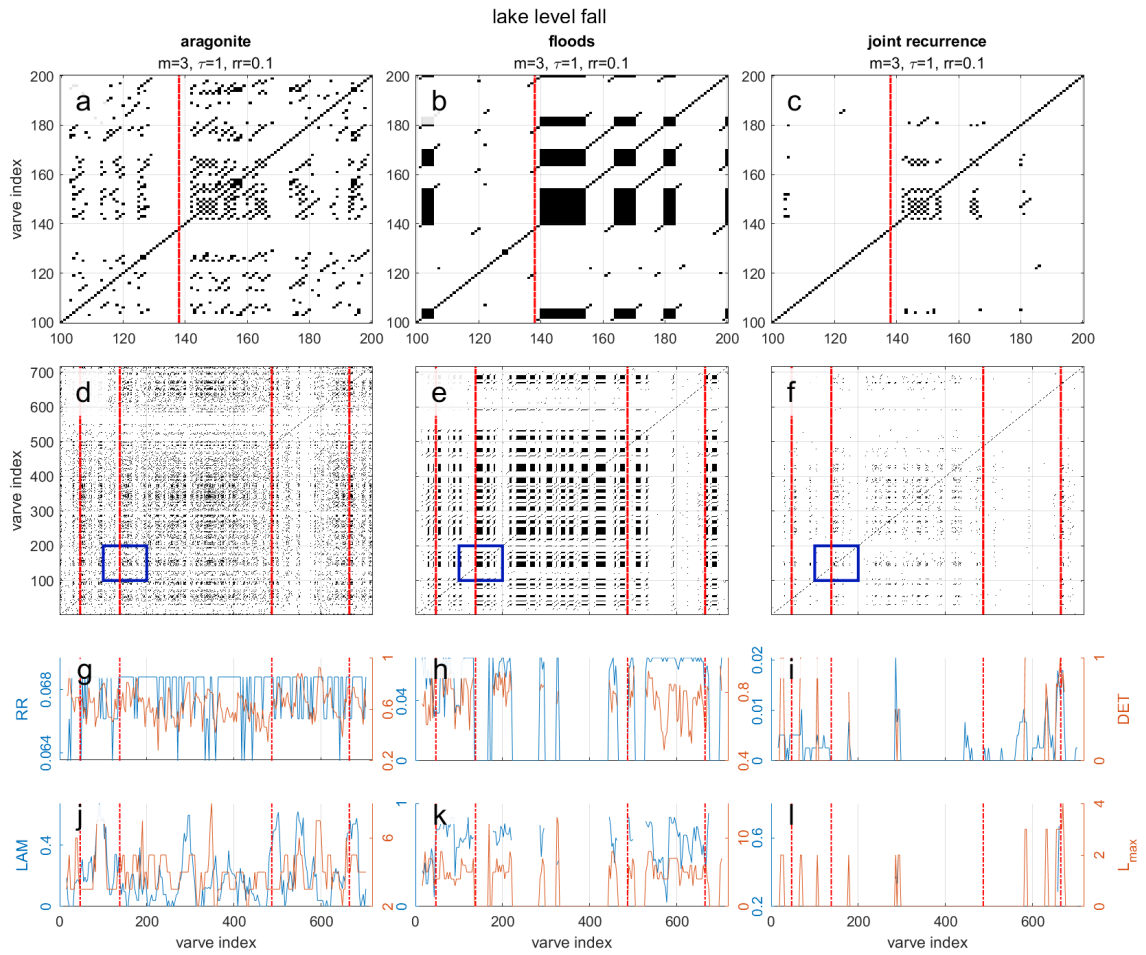
Figure 6 – (a-c) Enlarged segments of the recurrence plots of the studied lake level fall for aragonite thickness (a), flood frequency (b) and the joint recurrence plot for the two proxies (c). **(d-f)** Recurrence plots of the aragonite thickness (d), flood frequency (e) and the joint recurrence plot for the two proxies (f), with bue rectangles indicating the extent of data presented in (a-c). Note the parallel diagonal lines that characterize the aragonite thickness (a,d), and point on to an inherent oscillatory behaviour, whereas the flood series (b,e) forms sporadic points and polygons that reflect a more cahotic or random beviour. **(g-i)** The recurrence rate (*RR*) and the determinism (*DET*) coefficient using a running window size of 30 years and a single year step for aragonite thickness (g), floods (h) and the joint recurrence (i). . **(j-l)** The laminarity (*LAM*) and the maximum length of the diagonal line within the sub-matrix (*Lmax*) coefficient using a running window size of 30 years and a single year step for aragonite thickness (j), floods (k) and the joint recurrence (l). The analyses were carried over after detrending the data using the SSA RC[(1)]. Selected parametrs for the embedding are m (dimension), τ (delay) and ε (threshold) used for space phase reconstructions are presented in the figure. Red lines represent possible clusters identified indepently of the recurrence analyses.

Figure 7 – (a-c) Enlarged segments of the recurrence plots of the studied lake level rise for aragonite thickness (a), flood frequency (b) and the joint recurrence plot for the two proxies (c). (d-f) Recurrence plots of the aragonite thickness (d), flood frequency (e) and the joint recurrence plot for the two proxies (f), with bue rectangles indicating the extent of data presented in (a-c). Note the parallel diagonal lines that characterize the aragonite thickness (a,d), and point on to an inherent oscillatory behaviour, whereas the flood series (b,e) forms sporadic points and polygons that reflect a more cahotic or random beviour. (g-i) The recurrence rate (*RR*) and the determinism (*DET*) coefficient using a running window size of 30 years and a single year step for aragonite thickness (g), floods (h) and the joint recurrence (i). . (j-l) The laminarity (*LAM*) and the maximum length of the diagonal line within the sub-matrix (*Lmax*) coefficient using a running window size of 30 years and a single year step for aragonite thickness (j), floods (k) and the joint recurrence (l). The analyses were carried over after detrending the data using the SSA RC[(1)]. Selected parametrs for the embedding are m (dimension), τ (delay) and ε (threshold) used for space phase reconstructions are presented in the figure. Red lines represent possible clusters identified indepently of the recurrence analyses.

4.2 Detecting periodic components

Recurrence analyses of aragonite thicknesses indicate periodic or oscillatory behaviours, reflected by the appearance of diagonal lines in the recurrence plot of the series (Figs. 6 and 7). Conversely, the flood frequency series present blocky and

irregular patterns that indicate an underlying chaotic, random, or practically non-periodic process (Figs. 6 and 7). In particular, the segments identified as clusters demonstrate some abrupt changes in the studied RQA measures that could indicate a shift in the system's dynamics, both in aragonite thickness and in the number of sub-laminae. Although this behaviour is somewhat expected for the sub-laminae series that was used to determine clusters in the first place, it is also evident for the aragonite series.

Discontinuous short-term increased power of periodicities of the annual-decadal band appear sporadically throughout the entire dataset in both aragonite and flood frequency series (Fig. 8). However, these short-term oscillations are not significant with an $\alpha=0.05$, and additionally do not pass the global significance test. Instead, a couple of the significant patches that appear within this spectral band appear within clusters as vertically stretched patches that range over a set of periodicities ranging from sub-decadal to a multidecadal (30-60 years) frequency bands, which indicate that these periodicities are attributed to the abrupt pulse of increased variance occurring during the identified clusters (Hochman et al., 2019). These several significant patches pass the global significance test after detrending using the $RC^{(1)}$ of the SSA (Fig. S14). A centennial- to bicentennial band (~120-250 years) periodic component is observed in both aragonite thickness series, although its significance cannot be determined as it falls largely outside the cone of influence, and it fails the cumulative area-wise significance test. A similar periodic component is also identified in the sub-laminae series during lake level rise, but not in the interval of lake level fall. Altogether, the wavelet analyses do not suggest a robust detection of periodic components in any of the studied series.
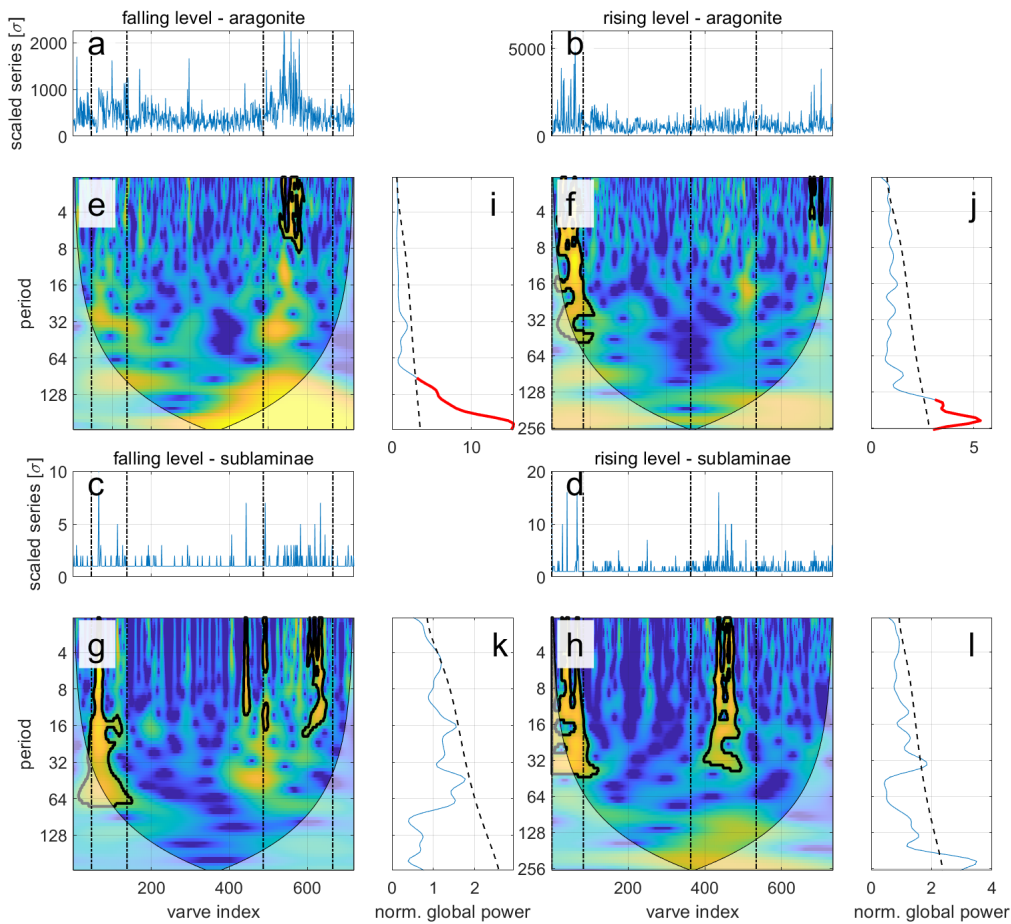
Figure 8 – Wavelet and global-wavelet spectra of aragonite thickness and flood frequency during falling (left) and rising (right) episodes. Periodicities with significance level above 0.95 (α=0.05) of the cumulative area-wise significance test are depicted by a bold black line (Schulte et al., 2018; Schulte, 2016). Each triplot section shows the normalized data (a-d), the wavelet spectra (e-h) and the global wavelet spectra (blue) compared against the significance test of the global wavelet power spectra (dashed black, i-l). Significant peaks of arcs are marked in red (Schulte, 2019). Vertical dashed lines in (e-h) depict clusters identified as episodes of increased flood frequency. Note that the short-term periodic component in the global wavelet spectra, which fail the significance of the series, are significant in the analysis of the detrended series (Fig. S14).

465   The SSA RCs are characterized by several periodic components (Figs. S10-S13). The first two components are considered as the local trend component, and accordingly depict persistent "long-wave" periodic components with wave lengths >32 years. The following components show roughly three peaks characterized by periodic components of sub-decadal frequencies.

5 Discussion

5.1 The mechanistic link between mean properties and variability

The poor correlation between aragonite thickness and the number of sub-laminae testifies to their low inter-dependence, and strengthen their interpretation as (nearly) independent proxies of the hydrological cycle in the Dead Sea watershed, in accordance with the previous interpretation of their roles in the hydrological cycle (Ben Dor et al., 2021; Ben Dor et al., 2018). Because of the unique hydroclimatic settings of the lake and its sedimentary record, the record cannot be directly interpreted from the perspective of a flood frequency analysis (e.g., Metzger et al., 2020), where the frequency and magnitude of floods in individual watersheds is analyzed. This is because detrital sub-laminae in the ICDP-DSDDP core record the number of flooding events, which potentially last up to several days (Nehorai et al., 2013), that exceeded the threshold required to reach the coring site at the lake depocenter (Ben Dor et al., 2018), instead of recording discharge properties at individual watersheds. Furthermore, the bathymetry of the basin dictates that only large-enough floods in tributaries situated in front of the coring site on both sides of the escarpment, could have deposited detrital material at the coring site (Fig. 1). Although this aspect masks some of the delicate features that could have been otherwise extracted such as in the analyses of modern measurements, its length and established context with respect to regional climatic conditions testifies to its value for interpreting hydroclimatic variability during episodes of climate change.

Available modern observations of sediment and water transport-paths into the lake, cannot unambiguously determine which synoptic systems affected the eastern Mediterranean when the studied sediment segments were deposited during the LGM. Nevertheless, considering available data that addresses this question, the likely suggestion that dominant weather regimes and synoptic circulation patterns during the LGM were similar to present is adopted for the sake of discussion in the framework of this work (Greenbaum et al., 2006; Amit et al., 2011; Enzel et al., 2008), with some possible modifications of their spatial properties (e.g., Goldsmith et al., 2017; Keinan et al., 2019). By considering that the dominant synoptic-scale circulation patterns during the late Pleistocene resemble modern observations in the region (Enzel et al., 2008), it can be argued that flooding events recorded as detrital sub-laminae at the depocenter of Lake Lisan can be attributed to the three key synoptic patterns that govern precipitation over the eastern Mediterranean (e.g., Armon et al., 2019). It is further suggested that the interplay and relative frequency of these three systems determine mean climatic conditions, that determine the Dead Sea lake level and ultimately propagate into its sedimentary record (Weber et al., 2021; Waldmann et al., 2017). Thus, the association of increased flood frequency with rising lake levels was interpreted as reflecting increased frequency and/or modulation of the Mediterranean Lows characteristics that deliver the majority of annual precipitation over the Dead Sea watershed, and hence determine annual inflow into the lake (Saaroni et al., 2010). However, a more detailed comparison of flood frequency with aragonite laminae thickness, that reflects annual inflow into the lake and the dilution of its epilimnion (Kolodny et al., 2005; Stein et al., 1997; Ben Dor et al., 2021), reveals more subtle insights and a delicate interplay of hydroclimatic factors manifested through the watershed during opposing climatic regimes.

Both aragonite laminae thickness and flood frequency have larger mean and variance during lake level rise (Table 1). Because rising lake levels indicate a "wetter-on-average" climate, this relationship between mean and variance is similar to that observed in modern hydrologic parameters such as precipitation (e.g., Morin et al., 2019). The observed relationship between the two studied proxies, thus, strengthens the interpretation of these sedimentary proxies as hydroclimatic proxies. Namely, the increased thickness of aragonite laminae and the increased number of detrital sub-laminae suggests that the episodes of rising lake level were characterized both by increased annual inflow and increased flood frequency. As suggestions invoking increased flood frequency were raised both for wetter and drier conditions were made (e.g., Alpert et al., 2002; Rohling, 2013; Yosef et al., 2019), this observation demonstrates that increased frequency of floods during wetter intervals in Mediterranean climate zones is the likely scenario. Furthermore, the observed coupling of increased thickness of aragonite laminae with increased flood frequency may support their formation by a common hydroclimatic mechanism, such as the increased occurrence of Mediterranean low pressure systems (Armon et al., 2019; Enzel et al., 2008; Ben Dor et al., 2018; Goldreich et al., 2004).

5.3 Periodic components and hydroclimatological pacing

One of the goals in studying hydroclimatological proxies is identifying key periodic components that pace short-term variability under different mean climatic regimes (e.g., Ghil et al., 2002; Grinsted et al., 2004). Because (a) the thickness of aragonite laminae was suggested to reflect hydroclimatic (Kolodny et al., 2005) and limnologic conditions (Ben Dor et al., 2021), and (b) periodicities attributed to solar cycles were previously identified by spectral analyses of laminae thickness at the coeval White Cliff Member outcrop the Lisan Formation at Masada deposited during MIS2 (Prasad et al., 2004), a similar attempt was made in this study identify similar periodic components as well. Prasad et al., (2004) report periodicities of 50-60 years, similar to those identified here (Figs. 8, S14). Additionally, previously reported $\delta^{18}O$ and $\delta^{13}C$ from ~200 aragonite laminae recovered from MIS2 exposures of the Lisan Formation at Masada and Perazim Valley outcrops were analyzed using wavelet analyses. Because the systematics of these isotopic compositions are distinctly different, these proxies bear different implication on environmental conditions in the lake and its surroundings. More specifically, $\delta^{18}O$ is directly influenced by hydroclimatology, whereas $\delta^{13}C$ is primarily affected by biological activity (Kolodny et al., 2005). Nevertheless, it appears that because the extent of biological activity in Lake Lisan depended on freshwater inflow that also replenished its surface water with required nutrients (Begin et al., 2004), the two proxies share similar pacing and are broadly characterized by non-

530
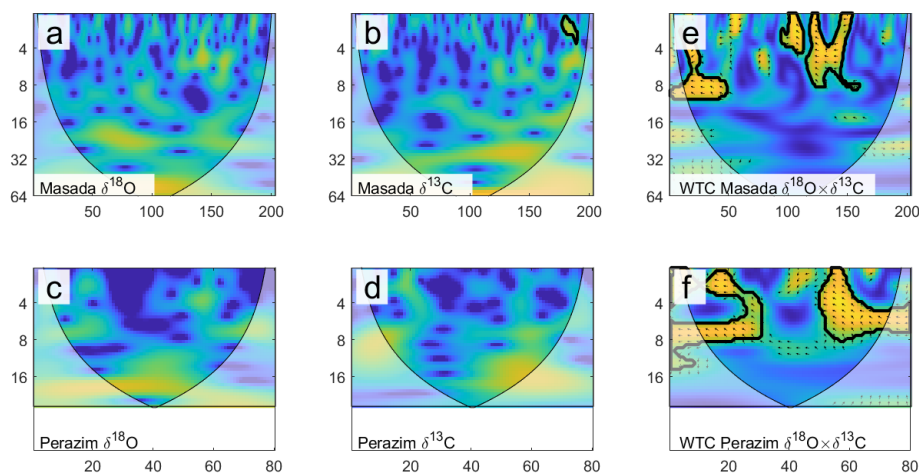
Figure 9 – Wavelet (a-d) and cross-wavelet (e-f) analyses of δ¹⁸O and δ¹³C in two segments of the Masada (30 Ka) and Perazim (25 Ka) exposures of the White Cliff Member (Lisan Formation) deposited during the last glacial over the lake's shelf. Areas with significance level above 0.95 (α=0.05) are marked by a thick black line. Data is from (Kolodny et al., 2005).

535

The North Atlantic oscillation (NAO) and the Eastern Atlantic (EA) patterns were considered to affect interannual precipitation variability over the eastern Mediterranean (Feldstein and Dayan, 2008; Feliks et al., 2010; Krichak et al., 2002; Seager et al., 2019), primarily due to their reported effect on discrete precipitation-bearing synoptic patterns over the eastern Mediterranean (e.g., Black, 2012). Other studies, on the other hand, have suggested that unlike western Turkey, NAO shows only minimal

540   direct impact on precipitation in the Levant, and that it might affect temperature instead (Enzel et al., 2003; Seager et al., 2020; Ziv et al., 2006). Although such relationships are hard to identify in geological records, a North Atlantic impact over the Dead Sea hydrology during the last glacial was identified by lake level reconstructions, where abrupt lake level drops took place during Heinrich events (Bartov et al., 2003). Additionally, a periodic component of a sub-decadal to decadal frequency bands (4-5, 7-8 and ~11 years) was also identified in laminated halite sequences deposited during the last interglacial and was

545   attributed to NAO (Palchan et al., 2017). However, modern observations, may indicate that this pacing is manifested by temperature variations, which bear determine halite deposition, rather than hydrologic forcing (Sirota et al., 2017, 2018).

Century-long precipitation data from the Kfar Giladi and Jerusalem stations correlate well with pre-regulated modern Dead Sea levels, and are thus considered as recorders of mean hydrological conditions over the northern and central parts of the

550   Dead Sea watershed in recent and past times (Enzel et al., 2003; Morin et al., 2019). Thus, available precipitation records in both stations were also compared to the winter (DJF) NAO and EA indices using wavelet and wavelet coherence in order to

detect common pacing and periodic components (Figs. S15 and S16; NOAA, 2020). These relatively short records are do not exhibit significant periodic components in the series, and no significant coherence as well. However, although the available records do not exhibit significant periodic behaviour (at α=0.05), increased non-significant spectral power of short-term fluctuations are evident in the ICDP-DSDDP cores (Figs. 8, S6, S10-S13), the isotopic composition of aragonite laminae (Fig. 9; Kolodny et al., 2005), and modern precipitation records and winter indices of teleconnection patterns (Figs. S15 and S16). This similarity that is not statistically significant, could either point at the lack of influence of NAO and EA on hydroclimate or at a weak and non-linear effect of these teleconnection patterns on precipitation in the eastern Mediterranean (Black, 2012). Alternatively, this can point at the inherent difficulties in extracting such delicate relationships from sedimentary archives that ultimately record the interaction of hydrological and limnological processes involved in laminae formation and post depositional changes, such as the non-homogenous spread of fine-grained sediments over the lake floor and the effects of inflows from different catchments.

5.3 Clusters and regime transitions

The studied episodes demonstrate pronounced centennial-scale clustering of flooding events (Fig. 3). Similarly, other high-resolution palaeo-hydrological records (e.g., Witt et al., 2017) and modern observations (e.g., Metzger et al., 2020) have demonstrated non-uniform and non-Poisson flood frequencies. In addition, the clusters observed during lake level fall are characterized by flood frequencies similar to those in background episodes during lake level rise (Figs. S17 and S18). This suggests that the wetter episodes are characterized by increased mean precipitation and variability, as well as increased frequency of intense storms, which is in agreement with modern and more recent observations (Morin et al., 2019).

The comparison of aragonite laminae thickness of the two clusters identified in each of the studied intervals reveals opposing properties, which become evident when comparing their RC$^{(1)}$ and dispersion, which is calculated as the running standard deviation of the residuals (after subtracting RC$^{(1)}$; Figs. 10 and 11). In each of the studied intervals, one cluster demonstrates increased mean and variance in both flood frequency and aragonite thickness, whereas the other cluster is characterized by increased mean flood frequency, but by mean and variance of aragonite thickness similar to that of background episodes (Figs. S17 and S18). In order to address these observations, a unified explanation that can account for this discrepancy is hereby suggested by considering the modern hydroclimatic regime and dominant synoptic circulation patterns.

Although modern records are relatively short, and the comparison of sparse hydrological measurements with the detailed framework of atmospheric circulation only permits cautious suggestions at this stage, the abovementioned observations can be explained using the modern synoptic framework by considering two distinct synoptic and hydroclimatic scenarios that govern flood generation and their clustering over the catchments that face the ICDP-DSDDP coring site. Most of the precipitation over the Dead Sea watershed is delivered by extra-tropical cyclones (Mediterranean lows) during the winter months (e.g., Enzel et al., 2003; Saaroni et al., 2010; Ziv et al., 2006). When these cyclones are deep and have a southern track,

585 their resulted precipitating clouds can pass impact the Dead Sea watershed for longer periods and generate more rainfall, and therefore effectively deliver more precipitation to the watershed (Ziv et al., 2006; Saaroni et al., 2010). Thus, under these conditions they increase annual precipitation, while increasing the chances of generating floods over the catchments that face the ICDP-DSDDP coring site (Armon et al., 2019; Belachsen et al., 2017; Goldreich, 2004). As suggested above, this scenario could account for the observed coupled increase in both mean and variance of flood frequency and aragonite laminae thickness,

590 observed in one of the clusters in each of studied series (Fig. S17 and S18).
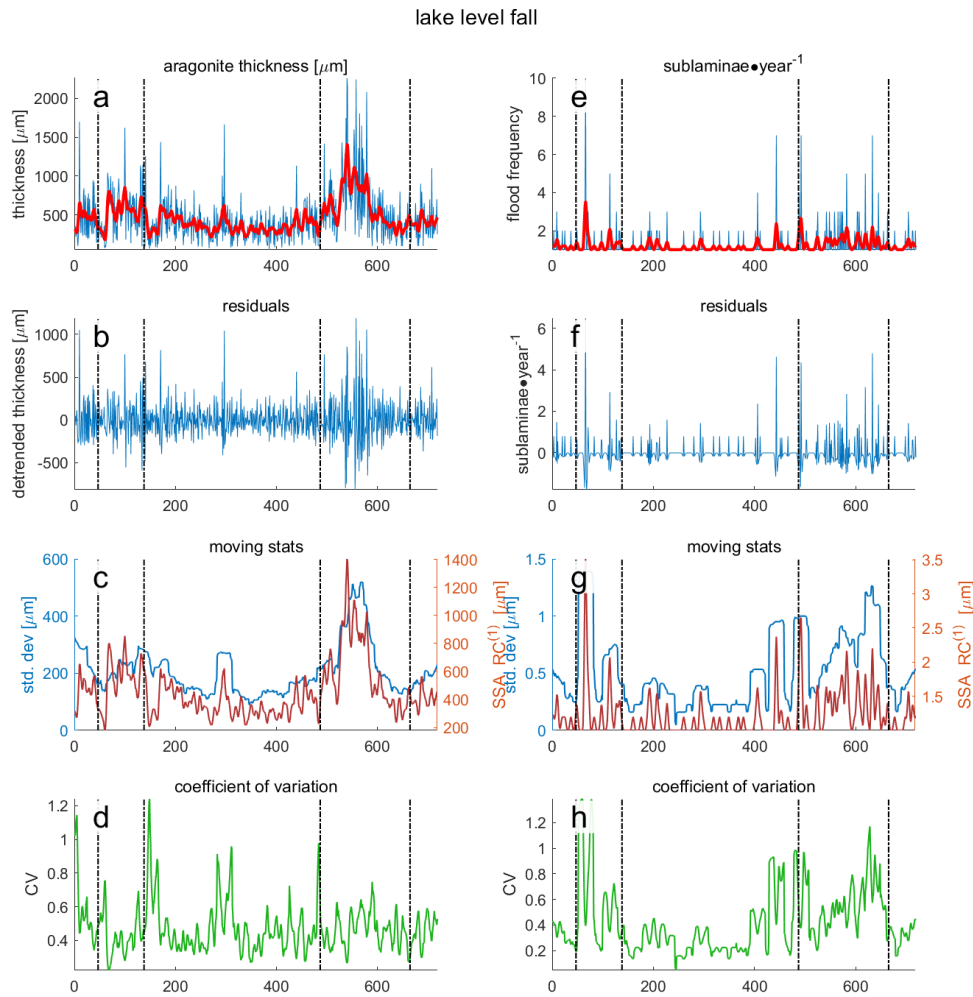
Figure 10 –running statistical properties of aragonite laminae (a-d) and flood frequency (e-h) for the studied lake level fall. (a,e) the measured data (b,f), the residuals (after subtracting the RC$^{(1)}$) (c,g), RC$^{(1)}$ and running std. deviation (30 years window), and the coefficient of variation calculated as $\frac{std}{RC^{(1)}}$ (d,h).

595   The general understanding of precipitation patterns induced by different synoptic systems in the Dead Sea watershed depicts a "de-coupling" of annual inflow into the lake, which depends on annual precipitation over the northern parts of the watershed, and floods reaching the coring site. This is because the frequency and intensity of (mainly *eastern) Mediterranean Lows* determines annual precipitation over the watershed (Saaroni et al., 2010) and flood frequency in the relevant ephemeral streams
600   (Goldreich et al., 2004), whereas the contribution of the other synoptic systems to annual precipitation by far, is less substantial (Armon et al., 2019; Marra et al., 2021). This is also evident by the low correlation ($r^2 = 0.086$) of major floods (return period >5 years) in the Negev Desert (Kahana et al., 2002) and precipitation in Jerusalem (Fig. R1), which found to be closely correlated with Dead Sea lake level, and hence with annual inflow into the lake (Enzel et al., 2003). Thus, although this cannot be directly proven for the LGM, these modern observations are hereby considered as means to decipher the sedimentary record
605   (e.g., Enzel et al., 2008; Goldsmith et al., 2017).

During the other cluster, on the other hand, the observed increased flood frequency is not coupled with increased mean and variance of aragonite laminae thickness. Studies of modern floods and their synoptic settings indicate that floods over the eastern Mediterranean are also generated by two other synoptic systems: the active Red Sea trough (ARST) and disturbances
610   to the subtropical jet stream (or Tropical Plumes). These synoptic conditions can generate significant floods over the small catchments surrounding the ICDP-DSDDP coring site, thus having the potential to deliver sediments, but owing to their spatiotemporal properties and frequency, they provide negligible contribution to total inflow into the lake (Armon et al., 2019). Under current conditions ARSTs are more frequent than Tropical Plumes, and are characterized by high peak discharge and relatively low volume floods (e.g., Armon et al., 2018; Shentsis et al., 2012) the second cluster may be therefore explained by
615   increased frequency of ARSTs during decades of decreased mean annual precipitation. This scenario would result in increased flood frequency, recorded by more sub-laminae, without substantially increasing annual inflow, thus exhibiting aragonite thicknesses similar to background periods.
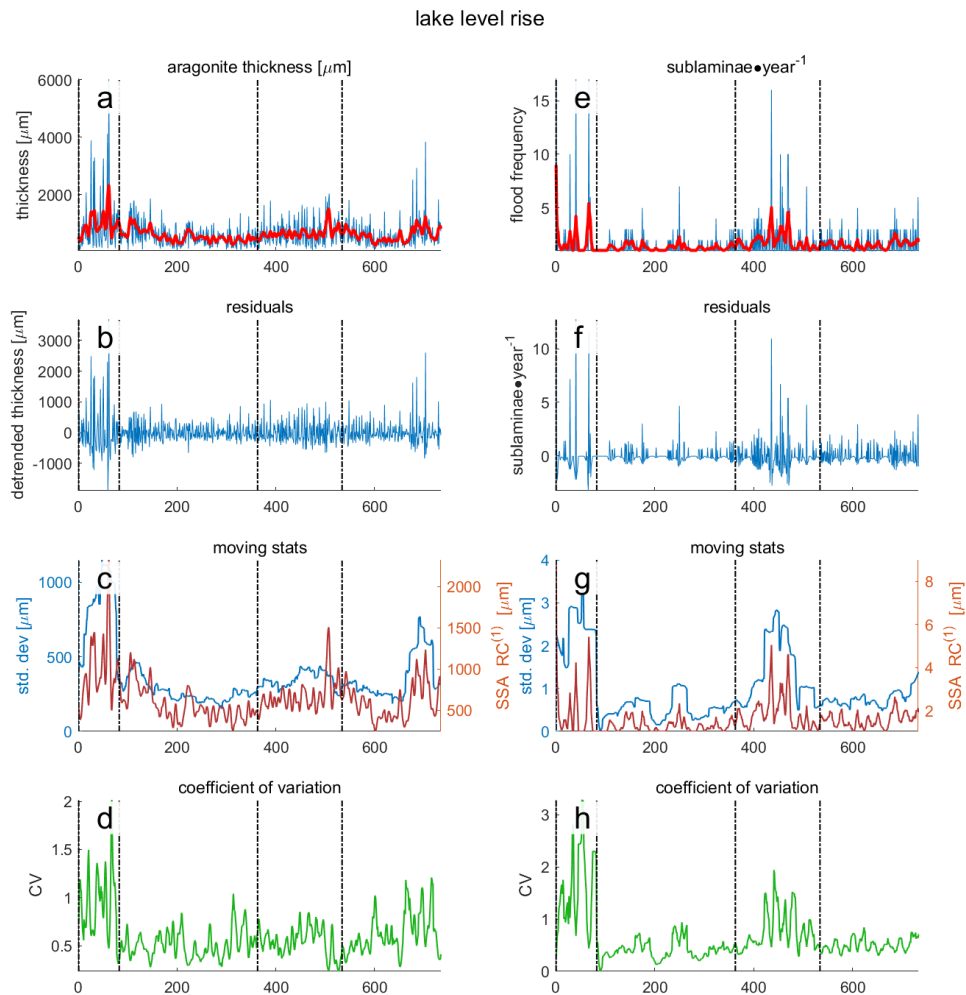
Figure 11 – running statistical properties of aragonite laminae (a-d) and flood frequency (e-h) for the studied lake level rise. (a,e) the measured data (b,f), the residuals (after subtracting the $RC^{(1)}$) (c,g), $RC^{(1)}$ and running std. deviation (30 years window), and the coefficient of variation calculated as $\frac{std}{RC^{(1)}}$ (d,h).

6 Conclusions

The short-term hydroclimatic variability of opposing climatic trends in the Levant was studied in detail through several analyses of two annually-resolved varve sequences of the ICDP-DSDDP cores, representing opposing mean climates recorded by contrasting lake level trends. This unique sedimentary record complements the otherwise short and sparse modern climatic and hydrological records, and elucidates aspects and properties of regional hydroclimatology on centennial time scale. By the

analyses of two sedimentary proxies that reflect annual inflow and flood frequency, and by their comparison with modern climatic data and synoptic observations, new insights on hydroclimatic stationarity during late Pleistocene climate changes were revealed. These findings improve our understanding of short-term late Pleistocene hydroclimatic variability.

Key conclusions arise:

630   1. The dispersion of aragonite laminae thickness and flood frequency in the ICDP-DSDDP cores change with their mean, as observed in modern hydrologic observations. These findings strengthen the interpretation of these proxies as recorders of hydroclimatic phenomena in the Dead Sea watershed. During the "wetter" interval, which is characterized by lake level rise, both the mean and the variance of these proxies are larger than during the studied episode of falling lake level.

635   2. No significant periodic components were identified in the studied records using singular spectrum, wavelet and recurrence analyses. However, it is suggested that this could stem from the interaction of climatic, hydrologic, and limnogeological processes that may have increased the noise/signal ratio of the studied proxies. Thus, the integration of these methods suggest that some short-term oscillatory components could have affected annual precipitation and flood frequency during the late Pleistocene, but were not found to be significant.

640   3. Flood frequencies demonstrate hydro-climatological regime shifts operating at the centennial time scale. Floods are clustered into episodes of two distinct relationships between mean and dispersion of flood frequency and annual inflow. Namely, in each studied series one cluster is characterized by increased mean and variance of the two proxies, whereas the other cluster is characterized by increased mean and dispersion of flood frequency, but not in annual precipitation. This implies that the clusters were generated by a distinct hydroclimatic regime, that was characterized

645   by different dominance of synoptic circulation patterns that resulted in increased floods frequency at a decadal-scale, but without increasing annual precipitation. More specifically, it may suggest that clusters of increased flood frequencies could either result from the increased frequency of Mediterranean Lows or of Active Red Sea Troughs. Such regime shifts could also affect modern and future conditions that would manifest as drastic shifts at decadal to centennial scales.

650   **Code availability**

All code that was used for this research is available upon request from the corresponding author.

Data availability

All the data that was used for this research is available in the appendices or upon request from the corresponding author.

Competing interests

655 The authors declare that they have no conflict of interest.

Acknowledgements

This study is a contribution to the PALEX project "Paleohydrology and Extreme Floods from the Dead Sea ICDP core", funded by the DFG to A. Brauer, Y. Enzel, E. Morin, and Y. Erel (grant no. BR2208/13-1/-2). The authors acknowledge the support and contribution of laboratory staff and technicians in the GFZ, where preparation of thin-sections and photography were 660 carried. We thank J. Mingram, N. Nowaczyk, B. Brademann, F. Ott, N. Dräger and M. Köppel for technical support and fruitful discussions. Y.B. is also grateful for a scholarship from the Advanced School of Environmental Studies, the Hebrew University of Jerusalem, and from the Rieger Foundation-Jewish National Fund program for environmental studies.

References

Ahlborn, M., Armon, M., Ben Dor, Y., Neugebauer, I., Schwab, M. J., Tjallingii, R., Shoqeir, J. H., Morin, E., Enzel, 665 Y., and Brauer, A.: Increased frequency of torrential rainstorms during a regional late Holocene eastern Mediterranean drought, Quaternary Research, 89, 425-431, 10.1017/qua.2018.9, 2018.

Allen, K., Hope, P., Lam, D., Brown, J., and Wasson, R.: Improving Australia's flood record for planning purposes– can we do better?, Australasian Journal of Water Resources, 24, 36-45, 2020.
670

Alpert, P., Ben-Gai, T., Baharad, A., Benjamini, Y., Yekutieli, D., Colacino, M., Diodato, L., Ramis, C., Homar, V., Romero, R., Michaelides, S., and Manes, A.: The paradoxical increase of Mediterranean extreme daily rainfall in spite of decrease in total values, Geophysical Research Letters, 29, 31-31-31-34, 10.1029/2001GL013554, 2002.

Amit, R., Simhai, O., Ayalon, A., Enzel, Y., Matmon, A., Crouvi, O., Porat, N., and McDonald, E.: Transition from 675 arid to hyper-arid environment in the southern Levant deserts as recorded by early Pleistocene cummulic Aridisols, Quaternary Science Reviews, 30, 312-323, 2011.

Ansari, A. R. and Bradley, R. A.: Rank-sum tests for dispersions, The Annals of Mathematical Statistics, 31, 1174- 680 1189, 1960.

Armon, M., morin, E., and Enzel, Y.: Overview of modern atmospheric patterns controlling rainfall and floods into the Dead Sea: Implications for the lake's sedimentology and paleohydrology, Quaternary Science Reviews, 216, 58-73, 2019.

Armon, M., Dente, E., Smith, J. A., Enzel, Y., and Morin, E.: Synoptic-Scale Control over Modern Rainfall and Flood 685 Patterns in the Levant Drylands with Implications for Past Climates, Journal of Hydrometeorology, 19, 1077-1096, 10.1175/jhm-d-18-0013.1, 2018.

Armon, M., Marra, F., Enzel, Y., Rostkier-Edelstein, D., and Morin, E.: Radar-based characterisation of heavy 690 precipitation in the eastern Mediterranean and its representation in a convection-permitting model, Hydrology and Earth System Sciences, 24, 1227-1249, 2020.

Avni, S., Joseph-Hai, N., Haviv, I., Matmon, A., Benedetti, L., and Team, A.: Patterns and rates of 103–105 yr denudation in carbonate terrains under subhumid to subalpine climatic gradient, Mount Hermon, Israel, Bulletin, 131, 899-912, 2018.

Baker, V. R.: Paleoflood hydrology: Origin, progress, prospects, Geomorphology, 101, 1-13, 2008.

Bar-Matthews, M., Ayalon, A., Kaufman, A., and Wasserburg, G. J.: The Eastern Mediterranean paleoclimate as a reflection of regional events: Soreq cave, Israel, Earth Planet. Sci. Lett., 166, 85-95, 1999.

Bar-Matthews, M., Ayalon, A., Gilmour, M., Matthews, A., and Hawkesworth, C. J.: Sea–land oxygen isotopic relationships from planktonic foraminifera and speleothems in the Eastern Mediterranean region and their implication for paleorainfall during interglacial intervals, Geochim. Cosmochim. Acta, 67, 3181-3199, 2003.

Bartov, Y., Enzel, Y., Porat, N., and Stein, M.: Evolution of the Late Pleistocene–Holocene Dead Sea Basin from sequence statigraphy of fan deltas and lake-level reconstruction, Journal of Sedimentary Research, 77, 680-692, 2007.

Bartov, Y., Goldstein, S. L., Stein, M., and Enzel, Y.: Catastrophic arid episodes in the Eastern Mediterranean linked with the North Atlantic Heinrich events, Geology, 31, 439-442, 2003.

Bartov, Y., Stein, M., Enzel, Y., Agnon, A., and Reches, Z.: Lake levels and sequence stratigraphy of Lake Lisan, the Late Pleistocene precursor of the Dead Sea, Quaternary Research, 57, 9-21, 2002.

Begin, Z., Ehrlich, A., and Nathan, Y.: Lake Lisan: the Pleistocene precursor of the Dead Sea, Ministry of Commerce and Industry, Geological Survey of Israel, Jerusalem61, 45, 1974.

Begin, Z. B., Nathan, Y., and Ehrlich, A.: Stratigraphy and facies distribution in the Lisan Formation—new evidence from the area south of the Dead Sea, Israel, Israel Journal of Earth Sciences, 29, 182-189, 1980.

Begin, Z. B., Stein, M., Katz, A., Machlus, M., Rosenfeld, A., Buchbinder, B., and Bartov, Y.: Southward migration of rain tracks during the last glacial, revealed by salinity gradient in Lake Lisan (Dead Sea rift), Quaternary Science Reviews, 23, 1627-1636, 10.1016/j.quascirev.2004.01.002, 2004.

Belachsen, I., Marra, F., Peleg, N., and Morin, E.: Convective rainfall in dry climate: relations with synoptic systems and flash-flood generation in the Dead Sea region, Hydrol. Earth Syst. Sci. Discuss, 2017.

Belmaker, R., Taha, N., and Bookman, R.: Evidence for aragonite deposition in flood plumes of the Dead Sea, Goldschmidt Abstract 196,

Belmaker, R., Lazar, B., Stein, M., Taha, N., and Bookman, R.: Constraints on aragonite precipitation in the Dead Sea from geochemical measurements of flood plumes, Quaternary Science Reviews, 221, 105876, 2019.

Ben David-Novak, H., Morin, E., and Enzel, Y.: Modern extreme storms and the rainfall thresholds for initiating debris flows on the hyperarid western escarpment of the Dead Sea, Israel, Geological Society of America Bulletin, 116, 718-728, 2004.

Ben Dor, Y., Flax, T., Levitan, I., Enzel, Y., Brauer, A., and Erel, Y.: The paleohydrological implications of aragonite precipitation under contrasting climates in the endorheic Dead Sea and its precursors revealed by experimental investigations, Chemical Geology, 576, 10.1016/j.chemgeo.2021.120261, 2021.

Ben Dor, Y., Neugebauer, I., Enzel, Y., Schwab, M. J., Tjallingii, R., Erel, Y., and Brauer, A.: Varves of the Dead Sea sedimentary record, Quaternary Science Reviews, 215, 173-184, 2019.

745   Ben Dor, Y., Neugebauer, I., Enzel, Y., Schwab, M. J., Tjallingii, R., Erel, Y., and Brauer, A.: Reply to comment on Ben Dor Y. et al. "Varves of the Dead Sea sedimentary record." Quaternary Science Reviews 215 (2019): 173–184, Quaternary Science Reviews, 231, 10.1016/j.quascirev.2019.106063, 2020.

Ben Dor, Y., Armon, M., Ahlborn, M., Morin, E., Erel, Y., Brauer, A., Schwab, M. J., Tjallingii, R., and Enzel, Y.:
750   Changing flood frequencies under opposing late Pleistocene eastern Mediterranean climates, Sci Rep, 8, 8445, 10.1038/s41598-018-25969-6, 2018.

Black, E.: The influence of the North Atlantic Oscillation and European circulation regimes on the daily to interannual variability of winter precipitation in Israel, International Journal of Climatology, 32, 1654-1664, 2012.
755
Blackman, R. B. and Tukey, J. W.: The measurement of power spectra, 1958.

Bookman, R., Bartov, Y., Enzel, Y., and Stein, M.: Quaternary lake levels in the Dead Sea basin: two centuries of research, Geological Society of America Special Papers, 401, 155-170, 2006.
760
Brauer, A., Endres, C., and Negendank, J. F.: Lateglacial calendar year chronology based on annually laminated sediments from Lake Meerfelder Maar, Germany, Quaternary International, 61, 17-25, 1999.

Brauer, A., Mangili, C., Moscariello, A., and Witt, A.: Palaeoclimatic implications from micro-facies data of a 5900
765   varve time series from the Piànico interglacial sediment record, southern Alps, Palaeogeography, Palaeoclimatology, Palaeoecology, 259, 121-135, 2008.

Broomhead, D. S. and King, G. P.: Nonlinear phenomena and chaos, On the Qualitative Analysis of Experimental Dynamical Systems, Malvern science series, Bristol, UK, 113-144, 1986.
770
Campins, J., Genovés, A., Picornell, M., and Jansà, A.: Climatology of Mediterranean cyclones using the ERA-40 dataset, International Journal of Climatology, 31, 1596-1614, 2011.

Coianiz, L., Ben-Avraham, Z., Stein, M., and Lazar, M.: Spatial and temporal reconstruction of the late Quaternary
775   Dead Sea sedimentary facies from geophysical properties, Journal of Applied Geophysics, 160, 15-27, 2019.

Crouvi, O., Amit, R., Ben Israel, M., and Enzel, Y.: Loess in the Negev desert: sources, loessial soils, palaeosols, and palaeoclimatic implications, in: Quaternary of the Levant: Environments, Climate Change, and Humans. Cambridge University Press, Cambridge, edited by: Enzel, Y., and Bar-Yosef, O., 471-482, 2017.
780
Dayan, U. and Morin, E.: Flash flood–producing rainstorms over the Dead Sea: A review, Geological Society of America Special Papers, 401, 53-62, 2006.

Dean, J. R., Eastwood, W. J., Roberts, N., Jones, M. D., Yiğitbaşıoğlu, H., Allcock, S. L., Woodbridge, J., Metcalfe,
785   S. E., and Leng, M. J.: Tracking the hydro-climatic signal from lake to sediment: A field study from central Turkey, Journal of Hydrology, 529, 608-621, 2015.

Donges, J. F., Donner, R. V., Trauth, M. H., Marwan, N., Schellnhuber, H.-J., and Kurths, J.: Nonlinear detection of paleoclimate-variability transitions possibly related to human evolution, Proceedings of the National Academy of Sciences,
790   108, 20422-20427, 2011.

Drori, R., Ziv, B., Saaroni, H., Etkin, A., and Sheffer, E.: Recent changes in the rain regime over the Mediterranean climate region of Israel, Climatic Change, 167, 15, 10.1007/s10584-021-03161-6, 2021.

795   Enzel, Y., Amit, R., Dayan, U., Crouvi, O., Kahana, R., Ziv, B., and Sharon, D.: The climatic and physiographic controls of the eastern Mediterranean over the late Pleistocene climates in the southern Levant and its neighboring deserts, Global and Planetary Change, 60, 165-192, 2008.

Enzel, Y., Bookman, R., Sharon, D., Gvirtzman, H., Dayan, U., Ziv, B., and Stein, M.: Late Holocene climates of the
800   Near East deduced from Dead Sea level variations and modern regional winter rainfall, Quaternary Research, 60, 263-273, 2003.

Enzel, Y., Amit, R., Grodek, T., Ayalon, A., Lekach, J., Porat, N., Bierman, P., Blum, J. D., and Erel, Y.: Late Quaternary weathering, erosion, and deposition in Nahal Yael, Israel: An "impact of climatic change on an arid watershed"?,
805   Bulletin, 124, 705-722, 2012.

Feldstein, S. B. and Dayan, U.: Circumglobal teleconnections and wave packets associated with Israeli winter precipitation, Quarterly Journal of the Royal Meteorological Society: A journal of the atmospheric sciences, applied meteorology and physical oceanography, 134, 455-467, 2008.
810
Feliks, Y., Ghil, M., and Robertson, A. W.: Oscillatory climate modes in the Eastern Mediterranean and their synchronization with the North Atlantic Oscillation, Journal of Climate, 23, 4060-4079, 2010.

Flocas, H. A., Simmonds, I., Kouroutzoglou, J., Keay, K., Hatzaki, M., Bricolas, V., and Asimakopoulos, D.: On
815   cyclonic tracks over the eastern Mediterranean, Journal of Climate, 23, 5243-5257, 2010.

Ganor, E. and Foner, H.: The mineralogical and chemical properties and the behaviour of aeolian Saharan dust over Israel, in: The impact of desert dust across the Mediterranean, Springer, 163-172, 1996.

820   Garber, R. A., Levy, Y., and Friedman, G. M.: The sedimentology of the Dead Sea, Carbonates and Evaporites, 2, 43-57, 1987.

Garfunkel, Z.: Internal structure of the Dead Sea leaky transform (rift) in relation to plate kinematics, Tectonophysics, 80, 81-108, 1981.
825
Garfunkel, Z. and Ben-Avraham, Z.: The structure of the Dead Sea basin, Tectonophysics, 266, 155-176, 1996.

Ghil, M., Allen, M., Dettinger, M., Ide, K., Kondrashov, D., Mann, M., Robertson, A. W., Saunders, A., Tian, Y., and Varadi, F.: Advanced spectral methods for climatic time series, Reviews of geophysics, 40, 2002.
830
Golan, R., Lazar, B., Wurgaft, E., Lensky, N., Ganor, J., and Gavrieli, I.: Continuous CO_2 escape from the hypersaline Dead Sea caused by aragonite precipitation, Geochim. Cosmochim. Acta, 207, 43-56, 10.1016/j.gca.2017.02.031, 2017.

835   Goldreich, Y.: Spatial Distribution of Mid-season Rainfall Date in Israel - a Review, Horizons in Geography, 177-182, 2004.

Goldreich, Y.: The climate of Israel: observation, research and application, Springer Science & Business Media2012.

840   Goldreich, Y., Mozes, H., and Rosenfeld, D.: Radar analysis of cloud systems and their rainfall yield in Israel, Isr. J. Earth Sci, 53, 63-76, 2004.

Goldsmith, Y., Polissar, P., Ayalon, A., Bar-Matthews, M., and Broecker, W.: The modern and Last Glacial Maximum hydrological cycles of the Eastern Mediterranean and the Levant from a water isotope perspective, Earth Planet. Sci. Lett., 457, 302-312, 2017.

Greenbaum, N., Schwartz, U., and Bergman, N.: Extreme floods and short-term hydroclimatological fluctuations in the hyper-arid Dead Sea region, Israel, Global and Planetary Change, 70, 125-137, 2010.

Greenbaum, N., Ben-Zvi, A., Haviv, I., and Enzel, Y.: The hydrology and paleohydrology of the Dead Sea tributaries, Geological Society of America Special Papers, 401, 63-93, 2006.

Grinsted, A., Moore, J. C., and Jevrejeva, S.: Application of the cross wavelet transform and wavelet coherence to geophysical time series, Nonlinear processes in geophysics, 11, 561-566, https://doi.org/10.5194/npg-11-561-2004, 2004.

Haase-Schramm, A., Goldstein, S. L., and Stein, M.: U-Th dating of Lake Lisan (late Pleistocene dead sea) aragonite and implications for glacial east Mediterranean climate change, Geochim. Cosmochim. Acta, 68, 985-1005, http://dx.doi.org/10.1016/j.gca.2003.07.016, 2004.

Heim, C., Nowaczyk, N. R., Negendank, J. F., Leroy, S. A., and Ben-Avraham, Z.: Near East desertification: evidence from the Dead Sea, Naturwissenschaften, 84, 398-401, 1997.

Held, I. M. and Soden, B. J.: Robust responses of the hydrological cycle to global warming, Journal of Climate, 19, 5686-5699, 2006.

Hochman, A., Saaroni, H., Abramovich, F., and Alpert, P.: Artificial Detection of Lower-Frequency Periodicity in Climatic Studies by Wavelet Analysis Demonstrated on Synthetic Time Series, Journal of Applied Meteorology and Climatology, 58, 2077-2086, 2019.

IPCC, Zhai, V. P., Pirani, A. S., Connors, L., Péan, C., Berger, S., Caud, N., Chen, Y., Goldfarb, L., Gomis, M. I., Huang, M., Leitzell, K., Lonnoy, J. B. E., Matthews, R., Maycock, T. K., Waterfield, T., Yelekçi, O., Yu, R., and Zhou, B. (Eds.): Climate Change 2021: The Physical Science Basis, Cambridge University Press. In Press2021.

Kagan, E., Stein, M., and Marco, S.: Integrated Paleoseismic Chronology of the Last Glacial Lake Lisan: From Lake Margin Seismites to Deep-Lake Mass Transport Deposits, Journal of Geophysical Research: Solid Earth, 10.1002/2017JB014117, 2018.

Kahana, R., Ziv, B., Enzel, Y., and Dayan, U.: Synoptic climatology of major floods in the Negev Desert, Israel, International Journal of Climatology, 22, 867-882, 2002.

Kalderon-Asael, B., Erel, Y., Sandler, A., and Dayan, U.: Mineralogical and chemical characterization of suspended atmospheric particles over the east Mediterranean based on synoptic-scale circulation patterns, Atmospheric Environment, 43, 3963-3970, 2009.

Katz, A., Kolodny, Y., and Nissenbaum, A.: The geochemical evolution of the Pleistocene Lake Lisan-Dead Sea system, Geochim. Cosmochim. Acta, 41, 1609-1626, 10.1016/0016-7037(77)90172-7, 1977.

Kaufman, A.: U-Series dating of Dead Sea Basin carbonates, Geochim. Cosmochim. Acta, 35, 1269-1281, http://dx.doi.org/10.1016/0016-7037(71)90115-3, 1971.

Keinan, J., Bar-Matthews, M., Ayalon, A., Zilberman, T., Agnon, A., and Frumkin, A.: Paleoclimatology of the Levant from Zalmon Cave speleothems, the northern Jordan Valley, Israel, Quaternary Science Reviews, 220, 142-153, 2019.

895   Kelley, C., Ting, M., Seager, R., and Kushnir, Y.: Mediterranean precipitation climatology, seasonal cycle, and trend as simulated by CMIP5, Geophysical Research Letters, 39, 2012.

Kennel, M. B., Brown, R., and Abarbanel, H. D.: Determining embedding dimension for phase-space reconstruction using a geometrical construction, Physical review A, 45, 3403, 1992.

900   Kitagawa, H., Stein, M., Goldstein, S. L., Nakamura, T., and Lazar, B.: Radiocarbon chronology of the DSDDP core at the deepest floor of the Dead Sea, Radiocarbon, 59, 383-394, 10.1017/RDC.2016.120, 2017.

Kolodny, Y., Stein, M., and Machlus, M.: Sea-rain-lake relation in the Last Glacial East Mediterranean revealed by $\delta18O$-$\delta13C$ in Lake Lisan aragonites, Geochim. Cosmochim. Acta, 69, 4045-4060, 10.1016/j.gca.2004.11.022, 2005.
905   Kondrashov, D. and Ghil, M.: Spatio-temporal filling of missing points in geophysical data sets, Nonlinear Processes in Geophysics, 13, 151-159, 2006.

Kottek, M., Grieser, J., Beck, C., Rudolf, B., and Rubel, F.: World map of the Köppen-Geiger climate classification
910   updated, Meteorologische Zeitschrift, 15, 259-263, 2006.

Krichak, S., Kishcha, P., and Alpert, P.: Decadal trends of main Eurasian oscillations and the Eastern Mediterranean precipitation, Theoretical and Applied Climatology, 72, 209-220, 2002.

915   Kushnir, Y., Dayan, U., Ziv, B., Morin, E., and Enzel, Y.: Climate of the Levant, in: Quaternary of the Levant, edited by: Enzel, Y., and Bar-Yosef, O., Cambridge University Press, Cambridge, 31-44, 10.1017/9781316106754.004, 2017.

Lau, K. and Weng, H.: Climate signal detection using wavelet transform: How to make a time series sing, Bulletin of the American Meteorological Society, 76, 2391-2402, 1995.
920   Le Mouël, J. L., Lopes, F., and Courtillot, V.: A Solar Signature in Many Climate Indices, Journal of Geophysical Research: Atmospheres, 2019.

Levy, Y., Burg, A., Yechieli, Y., and Gvirtzman, H.: Displacement of springs and changes in groundwater flow
925   regime due to the extreme drop in adjacent lake levels: The Dead Sea rift, Journal of Hydrology, 587, 10.1016/j.jhydrol.2020.124928, 2020.

Lisiecki, L. E. and Raymo, M. E.: A Pliocene-Pleistocene stack of 57 globally distributed benthic $\delta18O$ records, Paleoceanography, 20, 2005.
930   Luck, M., Landis, M., and Gassert, F.: Aqueduct water stress projections: decadal projections of water supply and demand using CMIP5 GCMs, Technical Note. Washington, DC: World Resources Institute. Available online at: http://www. wri. org/publication/aqueduct-waterstress-projections, 2015.

935   Luo, T., Young, R., and Reig, P.: Aqueduct Projected Water Stress Country Rankings, Technical Note, 2015.

Machlus, M., Enzel, Y., Goldstein, S. L., Marco, S., and Stein, M.: Reconstructing low levels of Lake Lisan by correlating fan-delta and lacustrine deposits, Quaternary International, 73, 137-144, 2000.

940   Mann, H. B. and Whitney, D. R.: On a test of whether one of two random variables is stochastically larger than the other, The annals of mathematical statistics, 50-60, 1947.

Marco, S., Stein, M., Agnon, A., and Ron, H.: Long-term earthquake clustering: A 50,000-year paleoseismic record in the Dead Sea Graben, Journal of Geophysical Research: Solid Earth, 101, 6179-6191, 1996.
945

Marra, F., Armon, M., Adam, O., Zoccatelli, D., Gazal, O., Garfinkel, C. I., Rostkier-Edelstein, D., Dayan, U., Enzel, Y., and Morin, E.: Toward Narrowing Uncertainty in Future Projections of Local Extreme Precipitation, Geophysical Research Letters, 48, e2020GL091823, 2021.

950   Marwan, N.: How to avoid potential pitfalls in recurrence plot based data analysis, International Journal of Bifurcation and Chaos, 21, 1003-1017, 2011.

Marwan, N. and Kurths, J.: Cross recurrence plots and their applications, Mathematical physics research at the cutting edge, 101-139, 2004.
955

Marwan, N., Romano, M. C., Thiel, M., and Kurths, J.: Recurrence plots for the analysis of complex systems, Physics reports, 438, 237-329, 2007.

Marwan, N., Trauth, M. H., Vuille, M., and Kurths, J.: Comparing modern and Pleistocene ENSO-like influences in 960   NW Argentina using nonlinear time series analysis methods, Climate Dynamics, 21, 317-326, 2003.

Metzger, A., Marra, F., Smith, J. A., and Morin, E.: Flood frequency estimation and uncertainty in arid/semi-arid regions, Journal of Hydrology, 590, 125254, 2020.

965   Migowski, C., Stein, M., Prasad, S., Negendank, J. F., and Agnon, A.: Holocene climate variability and cultural evolution in the Near East from the Dead Sea sedimentary record, Quaternary Research, 66, 421-431, 2006.

Morin, E.: To know what we cannot know: Global mapping of minimal detectable absolute trends in annual precipitation, Water Resources Research, 47, 2011.
970

Morin, E., Ryb, T., Gavrieli, I., and Enzel, Y.: Mean, variance, and trends of Levant precipitation over the past 4500 years from reconstructed Dead Sea levels and stochastic modeling, Quaternary Research, 91, 751-767, 2019.

Neev, D.: Recent precipitation of calcium salts in the Dead Sea, Bull. Res. Council Israel, Sect. G, 11, 153-154, 1963.
975

Neev, D. and Emery, K. O.: The Dead Sea: depositional processes and environments of evaporites, Ministry of Commerce and Industry, Geological Survey of Israel, Jerusalem, 1967.

Nehorai, R., Lensky, I., Hochman, L., Gertman, I., Brenner, S., Muskin, A., and Lensky, N.: Satellite observations of 980   turbidity in the Dead Sea, Journal of Geophysical Research: Oceans, 118, 3146-3160, 2013.

Neugebauer, I., Brauer, A., Schwab, M. J., Dulski, P., Frank, U., Hadzhiivanova, E., Kitagawa, H., Litt, T., Schiebel, V., and Taha, N.: Evidences for centennial dry periods at~ 3300 and~ 2800 cal. yr BP from micro-facies analyses of the Dead Sea sediments, The Holocene, 0959683615584208, 2015.
985

Neugebauer, I., Brauer, A., Schwab, M. J., Waldmann, N. D., Enzel, Y., Kitagawa, H., Torfstein, A., Frank, U., Dulski, P., and Agnon, A.: Lithology of the long sediment record recovered by the ICDP Dead Sea Deep Drilling Project (DSDDP), Quaternary Science Reviews, 102, 149-165, 2014.

Nissenbaum, A., Baedecker, M. J., and Kaplan, I. R.: Organic geochemistry of Dead Sea sediments, Geochim. Cosmochim. Acta, 36, 709-727, 1972.

NOAA Climate Prediction Center, teleconnection patterns, [dataset], 2020.https://www.cpc.ncep.noaa.gov/data/teledoc/telecontents.shtml

Palchan, D., Neugebauer, I., Amitai, Y., Waldmann, N. D., Schwab, M. J., Dulski, P., Brauer, A., Stein, M., Erel, Y., and Enzel, Y.: North Atlantic controlled depositional cycles in MIS 5e layered sediments from the deep Dead Sea basin, Quaternary Research, 87, 168-179, 2017.

Peleg, N., Bartov, M., and Morin, E.: CMIP5-predicted climate shifts over the East Mediterranean: implications for the transition region between Mediterranean and semi-arid climates, International journal of climatology, 35, 2144-2153, 2015.

Prasad, S., Negendank, J., and Stein, M.: Varve counting reveals high resolution radiocarbon reservoir age variations in palaeolake Lisan, Journal of Quaternary Science: Published for the Quaternary Research Association, 24, 690-696, 2009.

Prasad, S., Vos, H., Negendank, J., Waldmann, N., Goldstein, S. L., and Stein, M.: Evidence from Lake Lisan of solar influence on decadal-to centennial-scale climate variability during marine oxygen isotope stage 2, Geology, 32, 581-584, 2004.

Redmond, K. T., Enzel, Y., House, P. K., and Biondi, F.: Climate variability and flood frequency at decadal to millennial time scales, Ancient floods, modern hazards: principles and applications of paleoflood hydrology, 5, 21-45, 2002.

Roeser, P., Dräger, N., Brykała, D., Ott, F., Pinkerneil, S., Gierszewski, P., Lindemann, C., Plessen, B., Brademann, B., Kaszubski, M., Fojutowski, M., Schwab, M. J., Słowiński, M., Błaszkiewicz, M., and Brauer, A.: Advances in understanding calcite varve formation: new insights from a dual lake monitoring approach in the southern Baltic lowlands, Boreas, 10.1111/bor.12506, 2021.

Rohling, E. J.: Quantitative assessment of glacial fluctuations in the level of Lake Lisan, Dead Sea rift, Quaternary Science Reviews, 70, 63-72, 10.1016/j.quascirev.2013.03.013, 2013.

Romano, M. C., Thiel, M., Kurths, J., and von Bloh, W.: Multivariate recurrence plots, Physics letters A, 330, 214-223, 2004.

Ryb, U., Matmon, A., Erel, Y., Haviv, I., Benedetti, L., and Hidy, A.: Styles and rates of long-term denudation in carbonate terrains under a Mediterranean to hyper-arid climatic gradient, Earth Planet. Sci. Lett., 406, 142-152, 2014.

Saaroni, H., Halfon, N., Ziv, B., Alpert, P., and Kutiel, H.: Links between the rainfall regime in Israel and location and intensity of Cyprus lows, International Journal of Climatology, 30, 1014-1025, 2010.

Safriel, U., Adeel, Z., Niemeijer, D., Puigdefabregas, J., White, R., Lal, R., Winslow, M., Ziedler, J., Prince, S., and Archer, E.: Dryland systems, in: Ecosystems and Human Well-being: Current State and Trends.: Findings of the Condition and Trends Working Group, Island Press, 623-662, 2005.

Schinkel, S., Dimigen, O., and Marwan, N.: Selection of recurrence threshold for signal detection, The european physical journal special topics, 164, 45-53, 2008.

Schulte, J. A.: Cumulative areawise testing in wavelet analysis and its application to geophysical time series, Nonlinear Processes in Geophysics, 23, 45-57, 2016.

Schulte, J. A.: Statistical hypothesis testing in wavelet analysis: theoretical developments and applications to Indian rainfall, Nonlinear Processes in Geophysics, 26, 91-108, 2019.

Schulte, J. A., Georgas, N., Saba, V., and Howell, P.: North Pacific influences on Long Island sound temperature variability, Journal of Climate, 31, 2745-2769, 2018.

Seager, R., Osborn, T. J., Kushnir, Y., Simpson, I. R., Nakamura, J., and Liu, H.: Climate variability and change of Mediterranean-type climates, Journal of Climate, 32, 2887-2915, 2019.

Seager, R., Liu, H., Kushnir, Y., Osborn, T. J., Simpson, I. R., Kelley, C. R., and Nakamura, J.: Mechanisms of Winter Precipitation Variability in the European–Mediterranean Region Associated with the North Atlantic Oscillation, Journal of Climate, 33, 7179-7196, 2020.

Serinaldi, F., Kilsby, C. G., and Lombardo, F.: Untenable nonstationarity: An assessment of the fitness for purpose of trend tests in hydrology, Advances in Water Resources, 111, 132-155, 2018.

Israel Meteorological Service, Climatic data in Israel (1995-2009), [dataset], 2021.https://ims.gov.il/he/ClimateAtlas

Sharon, D.: The spottiness of rainfall in a desert area, Journal of Hydrology, 17, 161-175, 1972.

Sharon, D. and Kutiel, H.: The distribution of rainfall intensity in Israel, its regional and seasonal variations and its climatological evaluation, Journal of Climatology, 6, 277-291, 1986.

Shentsis, I., Laronne, J. B., and Alpert, P.: Red Sea Trough flood events in the Negev, Israel (1964–2007), Hydrological sciences journal, 57, 42-51, 2012.

Shohami, D., Dayan, U., and Morin, E.: Warming and drying of the eastern Mediterranean: Additional evidence from trend analysis, Journal of Geophysical Research: Atmospheres, 116, 2011.

Siebert, C., Rodiger, T., Mallast, U., Grabe, A., Guttman, J., Laronne, J. B., Storz-Peretz, Y., Greenman, A., Salameh, E., Al-Raggad, M., Vachtman, D., Zvi, A. B., Ionescu, D., Brenner, A., Merz, R., and Geyer, S.: Challenges to estimate surface- and groundwater flow in arid regions: the Dead Sea catchment, Sci Total Environ, 485-486, 828-841, 10.1016/j.scitotenv.2014.04.010, 2014.

Sirota, I., Enzel, Y., and Lensky, N. G.: Temperature seasonality control on modern halite layers in the Dead Sea: In situ observations, Geological Society of America Bulletin, B31661. 31661, 2017.

Sirota, I., Enzel, Y., and Lensky, N. G.: Halite focusing and amplification of salt layer thickness: From the Dead Sea to deep hypersaline basins, Geology, 2018.

Stein, M., Starinsky, A., Katz, A., Goldstein, S. L., Machlus, M., and Schramm, A.: Strontium isotopic, chemical, and sedimentological evidence for the evolution of Lake Lisan and the Dead Sea, Geochim. Cosmochim. Acta, 61, 3975-3992, 1997.

Stöckli, R., Vermote, E., Saleous, N., Simmon, R., and Herring, D.: The Blue Marble Next Generation-A true color earth dataset including seasonal dynamics from MODIS, Published by the NASA Earth Observatory, 2005.

Swierczynski, T., Brauer, A., Lauterbach, S., Martín-Puertas, C., Dulski, P., von Grafenstein, U., and Rohr, C.: A 1600 yr seasonally resolved record of decadal-scale flood variability from the Austrian Pre-Alps, Geology, 40, 1047-1050, 2012.

1090   Tamarin-Brodsky, T. and Kaspi, Y.: Enhanced poleward propagation of storms under climate change, Nature Geoscience, 10, 908, 2017.

Tarolli, P., Borga, M., Morin, E., and Delrieu, G.: Analysis of flash flood regimes in the North-Western and South-Eastern Mediterranean regions, Natural Hazards and Earth System Sciences, 12, 1255-1265, 2012.

1095   Torfstein, A. and Enzel, Y.: Dead Sea Lake Level Changes and Levant Palaeoclimate, in: Quaternary of the Levant, edited by: Enzel, Y., and Bar-Yosef, O., Cambridge University Press, Cambridge, 115-126, 10.1017/9781316106754.013, 2017.

1100   Torfstein, A., Goldstein, S. L., Kagan, E. J., and Stein, M.: Integrated multi-site U–Th chronology of the last glacial Lake Lisan, Geochim. Cosmochim. Acta, 104, 210-231, 2013a.

Torfstein, A., Goldstein, S. L., Stein, M., and Enzel, Y.: Impacts of abrupt climate changes in the Levant from Last Glacial Dead Sea levels, Quaternary Science Reviews, 69, 1-7, 2013b.

1105   Torfstein, A., Gavrieli, I., Katz, A., Kolodny, Y., and Stein, M.: Gypsum as a monitor of the paleo-limnological–hydrological conditions in Lake Lisan and the Dead Sea, Geochim. Cosmochim. Acta, 72, 2491-2509, 2008.

Torfstein, A., Haase-Schramm, A., Waldmann, N., Kolodny, Y., and Stein, M.: U-series and oxygen isotope 1110 chronology of the mid-Pleistocene Lake Amora (Dead Sea basin), Geochim. Cosmochim. Acta, 73, 2603-2630, 2009.

Torfstein, A., Goldstein, S. L., Kushnir, Y., Enzel, Y., Haug, G., and Stein, M.: Dead Sea drawdown and monsoonal impacts in the Levant during the last interglacial, Earth Planet. Sci. Lett., 412, 235-244, 2015.

1115   Torrence, C. and Compo, G. P.: A practical guide to wavelet analysis, Bulletin of the American Meteorological society, 79, 61-78, 1998.

Tsvieli, Y. and Zangvil, A.: Synoptic climatological analysis of 'wet'and 'dry'Red Sea troughs over Israel, International journal of climatology, 25, 1997-2015, 2005.

1120

Tubi, A. and Dayan, U.: Tropical Plumes over the Middle East: Climatology and synoptic conditions, Atmospheric Research, 145, 168-181, 2014.

Tyrlis, E., Lelieveld, J., and Steil, B.: The summer circulation over the eastern Mediterranean and the Middle East: 1125 influence of the South Asian monsoon, Climate Dynamics, 40, 1103-1123, 2013.

Vautard, R. and Ghil, M.: Singular spectrum analysis in nonlinear dynamics, with applications to paleoclimatic time series, Physica D: Nonlinear Phenomena, 35, 395-424, 1989.

1130   Waldmann, N., Neugebauer, I., Palchan, D., Hadzhiivanova, E., Taha, N., Brauer, A., and Enzel, Y.: Sedimentology of the Lacustrine Formations in the Dead Sea Basin, in: Quaternary of the Levant: Environments, Climate Change, and Humans, edited by: Enzel, Y., and Bar-Yosef, O., Cambridge University Press, Cambridge, 83-90, DOI: 10.1017/9781316106754.009, 2017.

1135   Weber, N., Lazar, B., Gavrieli, I., Yechieli, Y., and Stein, M.: Gypsum Deltas at the Holocene Dead Sea linked to Grand Solar Minima, Geophysical Research Letters, 10.1029/2020gl091034, 2021.

Welch, P. D.: The use of fast Fourier transform for the estimation of power spectra: A method based on time averaging over short, modified periodograms, IEEE Transactions on audio and electroacoustics, 15, 70-73, 1967.

1140

Witt, A., Malamud, B. D., Mangili, C., and Brauer, A.: Analysis and modelling of a 9.3 kyr palaeoflood record: correlations, clustering, and cycles, Hydrology and Earth System Sciences, 21, 5547-5581, 10.5194/hess-21-5547-2017, 2017.

Yosef, Y., Aguilar, E., and Alpert, P.: Changes in extreme temperature and precipitation indices: using an innovative 1145 daily homogenized database in Israel, International Journal of Climatology, 39, 5022-5045, 2019.

Zappa, G., Hoskins, B. J., and Shepherd, T. G.: The dependence of wintertime Mediterranean precipitation on the atmospheric circulation response to climate change, Environmental Research Letters, 10, 104012, 2015.

1150 Ziv, B.: A subtropical rainstorm associated with a tropical plume overAfrica and the Middle-East, Theoretical and Applied Climatology, 69, 91-102, 2001.

Ziv, B., Saaroni, H., and Alpert, P.: The factors governing the summer regime of the eastern Mediterranean, International Journal of Climatology, 24, 1859-1871, 2004.
1155

Ziv, B., Dayan, U., Kushnir, Y., Roth, C., and Enzel, Y.: Regional and global atmospheric patterns governing rainfall in the southern Levant, International Journal of Climatology, 26, 55-73, 2006.

Zolitschka, B., Francus, P., Ojala, A. E., and Schimmelmann, A.: Varves in lake sediments–a review, Quaternary 1160 Science Reviews, 117, 1-41, 2015.